

UNIVERSITÉ DE MONTRÉAL

POST-SURGE FLOW PREDICTION IN MULTI-STAGE COMPRESSORS

JAVAD HOSSEINI

DÉPARTEMENT DE GÉNIE MÉCANIQUE
ÉCOLE POLYTECHNIQUE DE MONTRÉAL

MÉMOIRE PRÉSENTÉ EN VUE DE L'OBTENTION
DU DIPLÔME DE MAÎTRISE ÈS SCIENCES APPLIQUÉES
(GÉNIE MÉCANIQUE)

AVRIL 2015

UNIVERSITÉ DE MONTRÉAL

ÉCOLE POLYTECHNIQUE DE MONTRÉAL

Ce mémoire intitulé :

PRÉDICTION D'ÉCOULEMENT DANS DES COMPRESSEURS MULTI-ÉTAGÉS DURANT
LE POMPAGE

présenté par : JAVAD HOSSEINI

en vue de l'obtention du diplôme de : Maîtrise ès sciences appliquées

a été dûment accepté par le jury d'examen constitué de :

M. MUREITHI Njuki, Ph. D., président

M. VO Huu Duc, Ph. D., membre et directeur de recherche

M. REGGIO Marcelo, Ph. D., membre

DEDICATION

To my family,

ACKNOWLEDGEMENTS

I would like to express my deepest appreciation to Prof. Huu Duc Vo for his guidance and support for me and my research.

I am grateful to my parents, my brother and my wife, who have continuously encouraged me in my study and in my life.

I worship my small children, their hands waiting to touch their daddy's hands who in return kisses their small hands when they sleep.

I would like to show my appreciation to the people who though their positive wishes always encouraged me.

I would like to express my gratitude to Prof. S. Rasouli who was my former advisor in undergraduate study.

I am thankful to my brilliant colleagues, Nouredine Djeghri, Farzad Ashrafi and Martial Dumas.

Last but not least, I would like to thank to all people who contribute their life to technological progress. The life we have today is the result of their endless effort.

RÉSUMÉ

Le pompage est une instabilité aérodynamique uni-dimensionnelle dans une turbine à gaz caractérisée par l'apparition de pulsations axiales allant jusqu'à une inversion globale du sens de l'écoulement et qui est très dommageable pour la performance de l'intégrité physique du moteur d'avion. La capacité de prédire les propriétés de l'écoulement pendant le pompage à différents endroits dans le compresseur aiderait les concepteurs à optimiser le design de plusieurs composantes du moteur pour mieux résister aux forces aérodynamiques impliquées.

L'objectif de cette recherche est de développer une méthode rapide et efficace pour prédire la fluctuation des propriétés de l'écoulement à n'importe quelle section dans un compresseur multi-étagés et qui serait utilisable au stage préliminaire de conception du moteur lorsque les détails sur la géométrie du compresseur sont encore limités. Suite à une revue de littérature sur les différentes méthodes pour simuler le pompage, une approche analytique a été choisie. La méthode développée dans ce projet est bâtie sur un modèle analytique de type *lumped-parameter* proposé il y a plus de trois décennies pour simuler le pompage dans des compresseurs axiaux de basse vitesse (écoulement incompressible). Ce modèle traitait le compresseur comme un *semi-actuator disk* à travers duquel l'augmentation de pression instantanée est obtenue à partir d'une courbe caractéristique en régime-permanent moins l'effet de l'inertie du fluide dans le compresseur. Le compresseur ainsi modélisé est couplé à un modèle 1-D des composantes en aval, soient un plenum pour la chambre à combustion et une valve pour la turbine. À travers ce travail, ce modèle a été amélioré en appliquant l'augmentation de pression en régime permanent et l'effet d'inertie du fluide aux sous-sections du compresseur pour facilement prédire les fluctuations de pression à l'intérieur du compresseur une fois que la prédiction du pompage pour le compresseur en entier ait été obtenue. La démonstration analytique de l'applicabilité de ce modèle aux compresseurs non-axiaux a été faite.

Ce modèle incompressible a été appliqué à trois géométries de compresseurs différentes pour lesquels des données expérimentales et/ou de simulations numériques de l'écoulement (CFD) pour le pompage sont disponibles. Ces géométries sont un compresseur axial de basse vitesse (incompressible) de trois étages, un compresseur axial-centrifuge de basse vitesse et un compresseur industriel non-axial bi-étagé de haute vitesse (régime hautement compressible). Les résultats montrent que ce modèle pourtant simple et rapide à préparer et à rouler performe assez

bien dans la prédiction de la forme du cycle de pompage, et de l'amplitude et la fréquence des fluctuations pour le compresseur en entier ainsi que pour un endroit à l'intérieur du compresseur (du moins pour le compresseur axial de basse vitesse) et ce, malgré les incertitudes dans l'estimation de la forme de la caractéristique du compresseur et la supposition d'incompressibilité.

ABSTRACT

Surge is a one-dimensional aerodynamic instability originating in the compressor of gas turbine engines. It is characterized by the appearance of axial fluctuations that can involve reversal of the flow throughout the engine. Surge is damaging both to the performance and the physical integrity of the engine. The ability to predict the flow properties during surge at different points inside the compressor will help designers optimize the design of engine components to better withstand the aerodynamic loads involved.

The objective of this research is to develop a rapid and efficient method to predict fluctuation in flow properties at any section inside a multi-stage compressor that can be used in the preliminary stage of the engine design where only limited information is available on the compressor geometry. Following a literature review of different methods for simulating surge, an analytical approach was chosen. The method developed in this project is built upon an analytical lumped-parameter model proposed over three decades ago to simulate surge in low-speed (incompressible flow) axial compressors. This model treated the compressor as a semi-actuator disk across which the instantaneous pressure rise is obtained from a steady-state pressure rise characteristic curve minus the effect of fluid inertia in the compressor. The modelled compressor is coupled with 1-D models for downstream components, namely a plenum representing the combustor and a throttle valve replacing the turbine. Through the current work, this model is enhanced by applying the same steady pressure rise and fluid inertia effect to subsections of the compressor to easily predict pressure oscillations inside the compressor once the surge prediction for the entire compressor has been obtained. This model is also shown analytically to be also applicable to non-axial compressors.

The incompressible model was applied on three different compressor geometries with available test and/or CFD surge data, namely a three-stage low-speed (incompressible) axial compressor, a low-speed axial-centrifugal compressor and an industrial high-speed two-stage (highly compressible) non-axial compressor. The results show that this simple model which is easy and fast to set up and run performs quite well in predicting the surge cycle shape, fluctuation amplitude and frequency for the overall compressor and for a location inside the compressor (at least on the low-speed axial compressor) in spite of uncertainty in speedline shape estimation and the incompressibility assumption.

TABLE OF CONTENTS

DEDICATION.....	III
ACKNOWLEDGEMENTS.....	IV
RÉSUMÉ.....	V
ABSTRACT.....	VII
TABLE OF CONTENTS.....	VIII
LIST OF TABLES.....	X
LIST OF FIGURES.....	XI
LIST OF SYMBOLS AND ABBREVIATIONS.....	XIV
LIST OF APPENDICES.....	XVII
CHAPTER 1 INTRODUCTION.....	1
1.1 Compressors.....	1
1.2 Aerodynamic Instabilities.....	4
1.3 Problem Definition.....	6
1.4 Objectives.....	7
1.5 Thesis Outline.....	8
CHAPTER 2 LITERATURE REVIEW.....	9
2.1 Analytical Methods.....	9
2.2 Computational Methods.....	14
CHAPTER 3 METHODOLOGY.....	18
3.1 General Strategy.....	18
3.2 Model Formulation.....	20
3.2.1 Compressor and Ducts.....	20
3.2.2 Plenum and Throttle.....	24

3.2.3	Surge Simulation	25
3.2.4	Surge Information Inside the Compressor	26
3.3	Analytical Model Assessment for Non-Axial Compressors	27
3.4	Compressor Geometries for Model Assessment	28
3.4.1	Low-Speed Axial Compressor	29
3.4.2	Low-Speed Axial-Centrifugal Compressor.....	32
3.4.3	High-Speed Compressor	33
3.5	Surge Simulation Procedure.....	34
CHAPTER 4	RESULTS	37
4.1	Low-Speed Axial Compressor (MIT-GTL LS3)	37
4.1.1	Surge Cycle Prediction for Compressor.....	37
4.1.2	Pressure Fluctuations Inside Compressor	40
4.2	Low-Speed Axial-Centrifugal Compressor.....	45
4.2.1	Surge Cycle Prediction for Compressor.....	45
4.2.2	Pressure Fluctuations Inside Compressor	47
4.3	High-Speed Compressor	48
4.4	Assessment of Speedline Shape and Density Effect	50
4.4.1	Sensitivity of Model to Speedline Shape	50
4.4.2	Sensitivity of Model to Density	51
CHAPTER 5	CONCLUSION AND RECOMMENDATIONS	53
BIBLIOGRAPHY	54
APPENDICES	57

LIST OF TABLES

Table 3.1: Parameters used for simulating surge of MIT-GTL LS3 compression system.....	32
Table 3.2: Parameters used for simulating surge of axial-centrifugal compression system.....	33
Table 3.3: Parameters used for simulating surge of high-speed compression system.....	34
Table B-1: Inertia components associated with blade rows and gaps for axial and centrifugal compressor stages in axial-centrifugal compressor.....	61

LIST OF FIGURES

Figure 1-1: Diagram of a typical gas turbine jet engine[1]	1
Figure 1-2: Axial compressor stage	2
Figure 1-3: Centrifugal compressor stage	3
Figure 1-4: Mixed flow compressor.....	3
Figure 1-5: Example of axial-centrifugal multi-stage compressor[2]	4
Figure 1-6: A schematic representation of a compressor map	5
Figure 1-7: Aerodynamic instabilities for a compressor	6
Figure 2-1: Schematic of Greitzer model[5]	10
Figure 2-2: Operating points from pressure matching between compressor and throttle (turbine)	10
Figure 2-3: Experimental validation of model by Greitzer[8]	11
Figure 2-4: Onset of surge for different plenum volume[8].....	12
Figure 2-5: Experimental results for two surge cycle with the same B parameter [8].....	12
Figure 2-6: Illustration of the methodology used by Dumas [6].....	16
Figure 2-7: Comparison of simulated surge cycle of low-speed axial compressor by Dumas with test data[6]	16
Figure 3-1: Example of proposed surge simulation strategy applied to a three-stage axial compressor	19
Figure 3-2: Schematic of compression system[13]	20
Figure 3-3: Blade passage approximation for calculating inertia effect	21
Figure 3-4: Modelling of plenum and throttle.....	24
Figure 3-5: Notation used in definition of (axisymmetric) compressor characteristics	26
Figure 3-6: Calculation of pressure at inquiry location inside compressor.....	26
Figure 3-7: Velocity triangle at the impeller tip.....	28

Figure 3-8: Schematic representation of the positions of the compressor blades and measurements of points for the MIT-GTL LS3 compressor [27]	30
Figure 3-9: Overview compressor MIT-GTL LS3 compressor [30].....	30
Figure 3-10: Surge cycle captured by Protz for the MIT GTL LS3 [28]	31
Figure 3-11: Modelled MIT GTL-LS3 compressor geometry (dimensions in m)	32
Figure 3-12: Schematic of low-speed axial-centrifugal compressor [30]	33
Figure 3-13: Layout of high-speed compressor	34
Figure 3-14: Operating point on speedline (a) and convergence history (b) for a stable value of K_T	35
Figure 3-15: Convergence history for K_T near or at critical value (stall point).....	35
Figure 3-16: Convergence history for K_T beyond critical value (surge)	36
Figure 4-1: Comparison of modelled speedline against experimental equivalent from Protz [28] for MIT-GTL LS3 compressor.....	38
Figure 4-2: Predicted versus measured surge cycles for MIT-GTL LS3 compressor	39
Figure 4-3: Predicted temporal variations in pressure rise and mass flow coefficients for MIT-GTL LS3 compressor (surge cycle frequency: 1.09 Hz)	39
Figure 4-4: Hot-wire velocity traces during surge cycle measured by Protz [28] (surge cycle frequency: 1.17 Hz).....	40
Figure 4-5: Comparison of modelled speedline against CFD equivalent from Dumas [6] for MIT-GTL LS3 compressor	41
Figure 4-6: Surge cycles predicted by model versus CFD [6] for MIT-GTL LS3 compressor with no ducts and $V_p = 3.66 \text{ m}^3$	42
Figure 4-7: Fluctuation in pressure rise and mass flow coefficients predicted by model (3.91 Hz) versus CFD (3.88 Hz) [6] for MIT-GTL LS3 compressor with no ducts and $V_p = 3.66 \text{ m}^3$...	43
Figure 4-8: Modelled pressure rise characteristics for last stage versus entire MIT-GTL LS3 compressor	44

Figure 4-9: Temporal variation of the pressure rise coefficient between stages 2 and 3 of MIT-GTL LS3 compressor during a surge cycle as predicted by the model and by CFD [6].	44
Figure 4-10: Comparison of modelled speedline against CFD equivalent from Dumas [6] for low-speed axial-centrifugal compressor	45
Figure 4-11: Surge cycles predicted by model versus CFD [6] for low-speed axial-centrifugal compressor	46
Figure 4-12: Fluctuation in pressure rise and mass flow coefficients predicted by model (1.53 Hz) versus CFD (1.78 Hz) [6] for low-speed axial-centrifugal compressor	46
Figure 4-13: Modelled pressure rise characteristics for low-speed axial-centrifugal compressor and its axial and radial components	47
Figure 4-14: Predicted temporal variation of the pressure rise coefficient between axial and centrifugal components of low-speed axial-centrifugal compressor.....	48
Figure 4-15: Estimation of cubic speedline based on surge cycle predicted by CFD from Dumas [6] for high-speed compressor.....	49
Figure 4-16: Surge cycles predicted by model versus CFD [6] for high-speed compressor	49
Figure 4-17: Fluctuation in pressure rise and mass flow coefficients predicted by model (12 Hz) versus CFD (10.61 Hz) [6] for high-speed compressor	50
Figure 4-18: Effect of speedline shape on surge cycle predictions for MIT-GTL LS3 compressor	51
Figure 4-19: Effect of density on surge fluctuation prediction for high-speed compressor	52
Figure A-1: Simulink blocks for solving surge ODEs	59
Figure B-1: Modelled flow path inside MIT-GTL LS3 compressor.....	60

LIST OF SYMBOLS AND ABBREVIATIONS

Variables

Latin

A	amplitude function of first-harmonic angular disturbance
A_c	compressor duct area
a	reciprocal time-lag parameter of blade passage
a_s	sound speed
B	$(U/2a_s)\sqrt{V_P / (A_c L_c)}$
b	chord length of a blade
C_m	meridional velocity
F	pressure-rise
F_T	throttle characteristic function, inverse is $F_T^{-1}(\Psi)$
f	nondimensional speed coefficient, relative to propagation of laboratory, of angular disturbance
f_0	value of f for single harmonic disturbance
g	disturbance of axial flow coefficient
H	semi-height of cubic axisymmetric characteristic
h	circumferential velocity coefficient
J	square of amplitude of angular disturbance of axial-flow coefficient; J_e for pure rotating stall
K_T	throttle coefficient
l_c	total aerodynamic length (L_c/R) of compressor and ducts, in wheel radii

l_E, l_I, l_T	length of exit, entrance, and throttle ducts, in wheel radii
m	compressor-duct flow parameter
N	number of stages of core compressor
P_S	pressure inside the plenum
p_0	static pressure at entrance to IGV
p_I, p_E	static pressures at entrance and exit of core compressor
p_S	static pressure at end of exit(diffuser) duct, and pressure in the plenum
p_T	total pressure ahead of entrance and following the throttle duct
R	mean wheel radius
r	time dependent phase angle
t	time
U	wheel speed at mean diameter
V_p	volume of plenum
W	semi width of cubic characteristic
Y	disturbance potential at compressor entrance
Greek	
η	axial distance measured in wheel radii
θ	angular coordinate around wheel
ξ	time, referred to time for wheel to rotate one radian
ρ	density
τ	coefficient of pressure rise lag
Φ	axial flow coefficient in compressor, annulus averaged; axial velocity divided by wheel speed
Φ_T	flow coefficient of throttle duct, referred to entrance-duct area
ϕ	local axial flow coefficient, a function of θ and ξ

$\tilde{\phi}$	velocity potential in entrance duct
$\tilde{\phi}^\circ$	disturbance velocity potential
Ψ	total to static pressure rise coefficient
Ψ_c	axisymmetric pressure rise coefficient
Ψ_{c0}	shut-off value of axisymmetric characteristic

Subscripts

0	at the entrance to the compressor
E	at the exit of the compressor

LIST OF APPENDICES

Appendix A – NUMERICAL IMPLEMENTATION.....	57
Appendix B – CALCULATION OF INERTIA PARAMETER.....	60

CHAPTER 1 INTRODUCTION

1.1 Compressors

The compressor is one of the three basic components of a gas turbine engine, along with the combustion chamber and the turbine, as illustrated in Figure 1-1. Its role is to compress the air that will then be heated through combustion and discharged through the turbine, whose work extraction is used to drive the compressor. The remaining exhaust gas is either accelerated through a nozzle to provide thrust or discharged through more turbines to produce mechanical power for driving aircraft/ship propellers, helicopter rotors or electrical generators. The compressor also serves to provide pressurized air, extracted at appropriate locations within it, for turbine cooling and, in aircraft applications, for cabin air climatization.

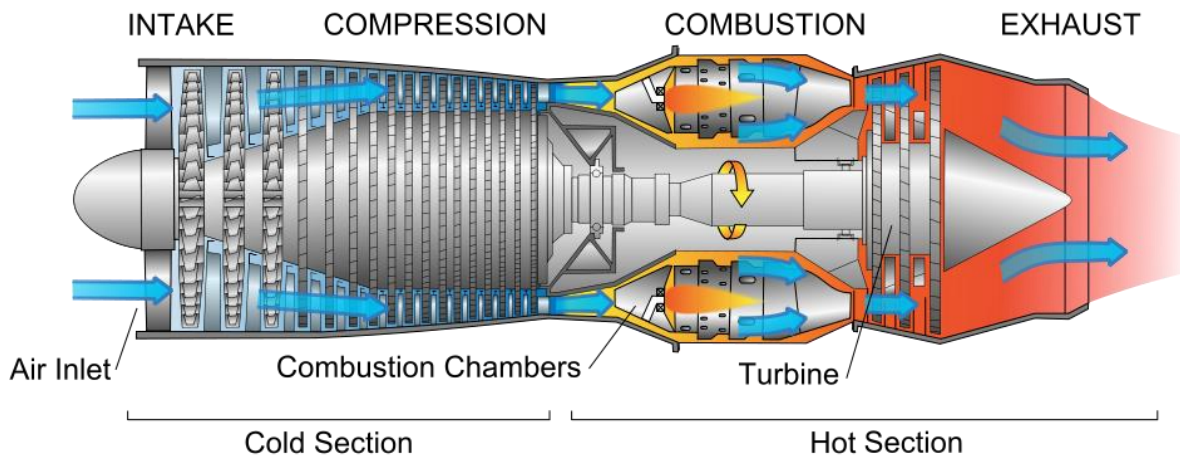


Figure 1-1: Diagram of a typical gas turbine jet engine[1]

A typical compressor stage is composed of a moving blade row followed by a stationary blade row. Two main types of compressors exist as defined by the change in mean radius of the flow from inlet to exit. When this change is minimal, it is an axial compressor and when it is important it is usually a centrifugal compressor. As shown in Figure 1-2, a rotor (moving blade row) redirects the flow in the relative frame thus increasing both static pressure through normal flow area increase and stagnation (total) pressure by increasing the flow velocity in the circumferential direction in the absolute frame. A stator (stationary blade row) redirects the flow toward the axial direction thus converting the increased kinetic energy into static pressure rise. For a centrifugal

compressor, shown in Figure 1-3, the moving blade row is an impeller which adds a lot more rotation to the flow, compared to an axial rotor, due to the large radius change from inlet to exit. At the same time, the centrifugal force from the rotation ensures a larger static pressure rise across the impeller than that across an axial rotor. However, the need for the diffuser to turn the high swirling flow exiting the impeller both circumferentially and radially back toward the axial direction results in higher pressure losses than in a stator. As a result, a centrifugal compressor stage provides several times more pressure rise than an axial stage but generally suffers from lower adiabatic efficiency and larger frontal area. A more seldom used type of compressor is the mixed flow compressor, which is essentially an axial stage with a large radius change in the rotor, as illustrated in Figure 1-4. It combines the effect of the axial centrifugal compressor, giving performances somewhere in-between.

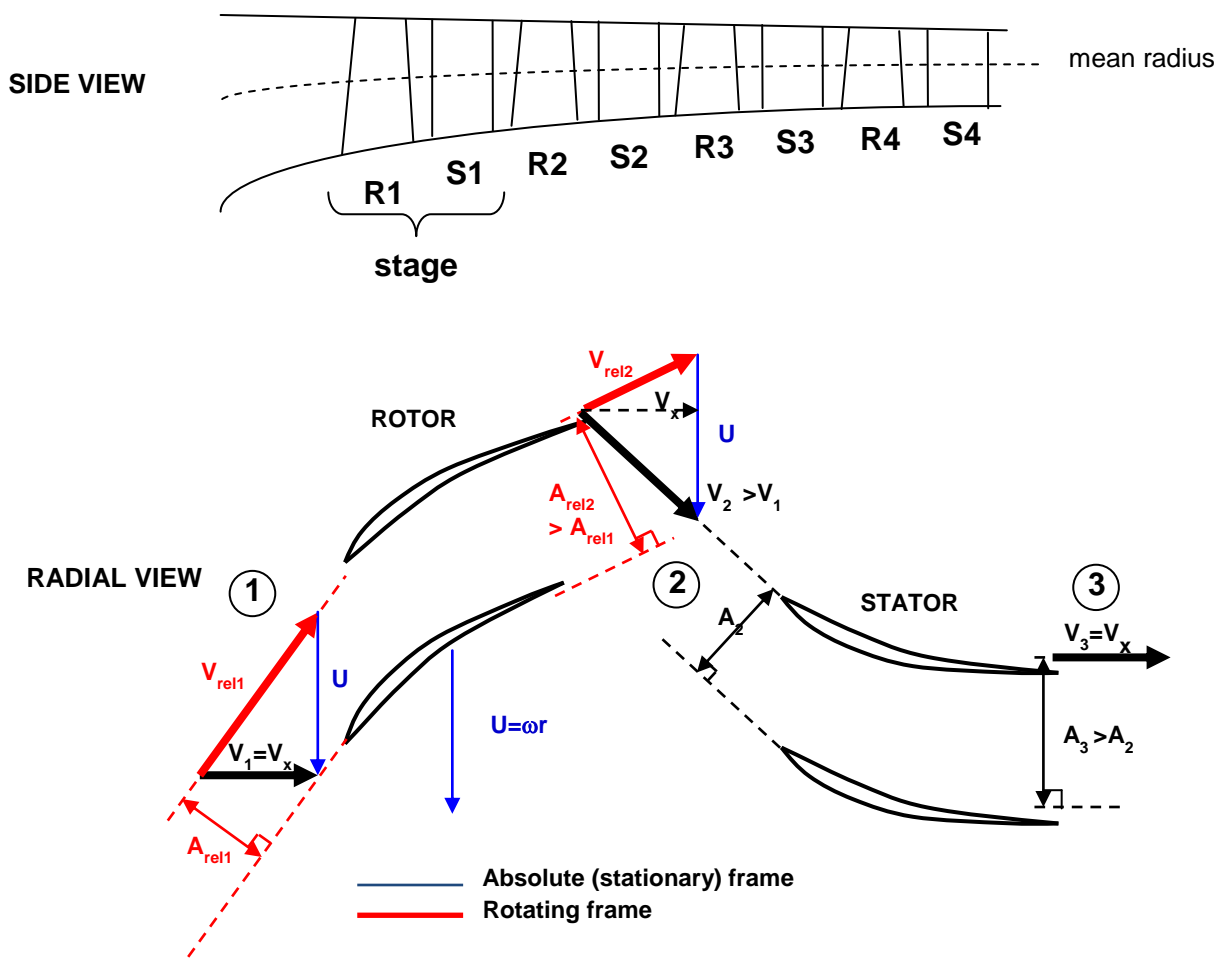


Figure 1-2: Axial compressor stage

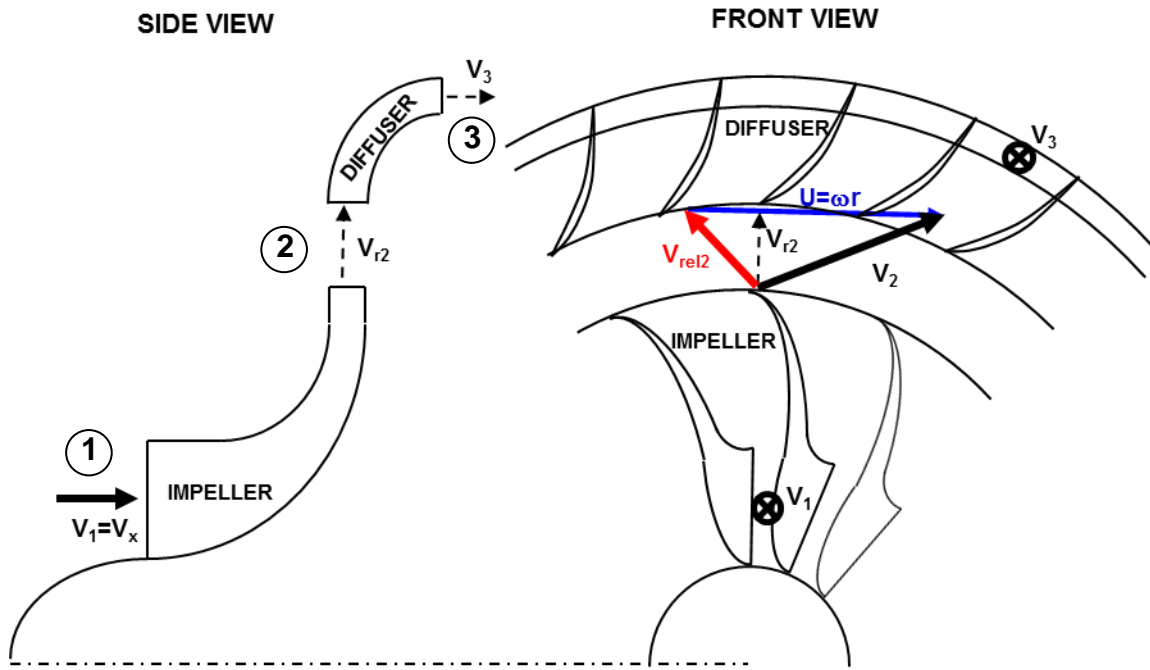


Figure 1-3: Centrifugal compressor stage

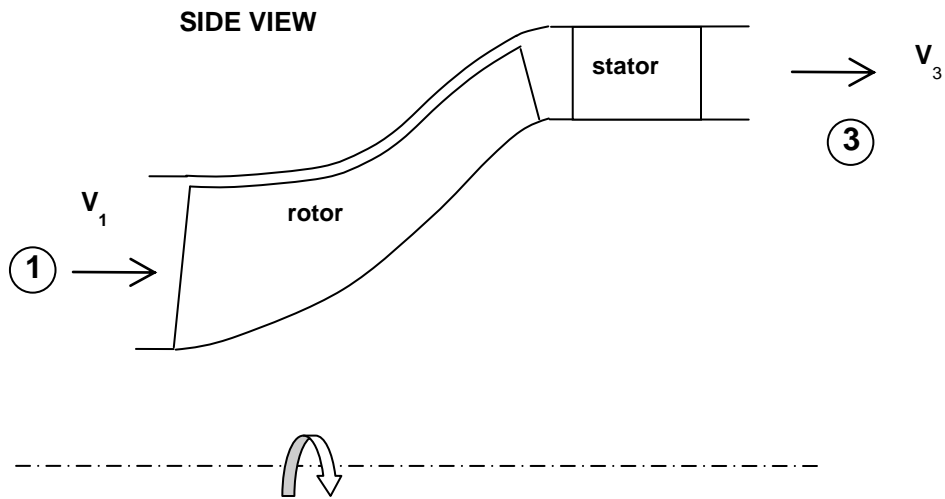


Figure 1-4: Mixed flow compressor

The compressor is arguably the most difficult component to design in a gas turbine from an aerodynamic stand point because it is essentially forcing the flow to go against a positive pressure gradient, making the blades susceptible to boundary layer separation. As such, the stage pressure ratio is limited and it requires many stages to achieve a required pressure ratio, making it the longest component of a gas turbine engine. In an aircraft application, where the number of compressor stages should be held to a minimum to limit engine length and weight, a combination of axial and centrifugal stages as shown in Figure 1-5 can sometime be used, especially in smaller engines where the rotational stresses of the smaller impellers can be kept reasonable, to minimize the number of stages without sacrificing too much in efficiency.

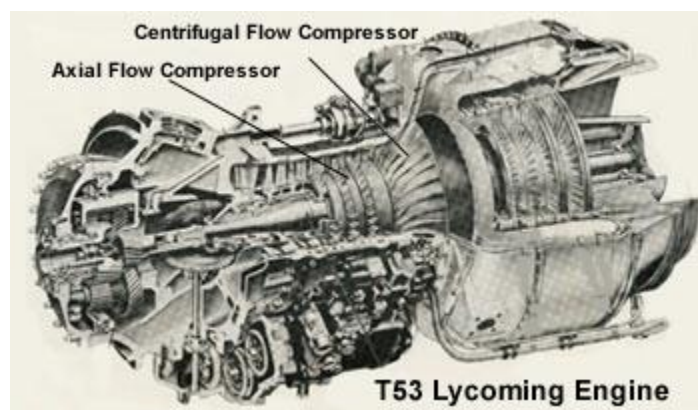


Figure 1-5: Example of axial-centrifugal multi-stage compressor[2]

1.2 Aerodynamic Instabilities

Figure 1-6 shows a typical compressor map in which each *speedline* represents the pressure rise versus mass flow at one particular rotation speed. As the mass flow decreases along a speedline, the axial velocity in Figure 1-2 increases, resulting in higher flow incidence and flow turning in the rotor and stator which increases pressure rise but also total pressure losses from among other things larger boundary layer growth on the blade/end wall surfaces from larger pressure gradients inside the blade passages. The increase in losses may lead the pressure rise to turn over as illustrated in Figure 1-6. Eventually, the speedline reaches an aerodynamic stability limit called *stall point* or *surge point* beyond which for example the blade boundary layer may separate. The line linking the stall/surge points of different speedlines is referred to as the *stall line* or the *surge line*.

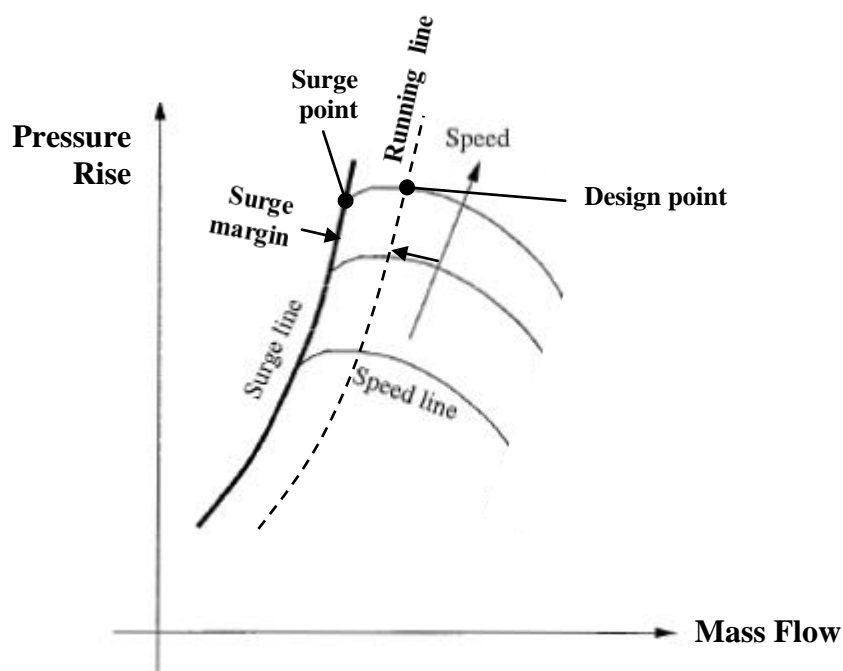


Figure 1-6: A schematic representation of a compressor map

At the stall/surge point, two types of aerodynamic instabilities can appear that are illustrated in Figure 1-7 for one particular speed. The first is rotating stall, which is characterized by the formation of a cell of velocity deficiency that rotates around the circumference at part of the rotor speed. By itself, rotating stall can cause a small drop in pressure rise (mild form) or a large drop in pressure rise (sever form) along the dashed line representing the combustor/turbine pressure drop characteristics intersecting the compressor speedline at the stall/surge point. However, in gas turbine applications, rotating stall usually triggers a much more severe instability called *surge*. Surge is an essentially axisymmetric flow oscillation across the entire gas turbine which in its most severe form (called *deep surge*), as illustrated in Figure 1-7, involves flow reversal across the compressor during part of the surge cycle. The link between rotating stall and surge can be intuitively understood as the inability of the compressor, once rotating stall occurs, to maintain the pressure inside the combustor leading to a partial discharge of the stored pressurized fluid and drop in combustor pressure until the compressor is able to pump flow anew, leading to

the surge cycle. Surge usually leads to a sudden and dramatic drop in engine power and damages to the engine and as such must be avoided.

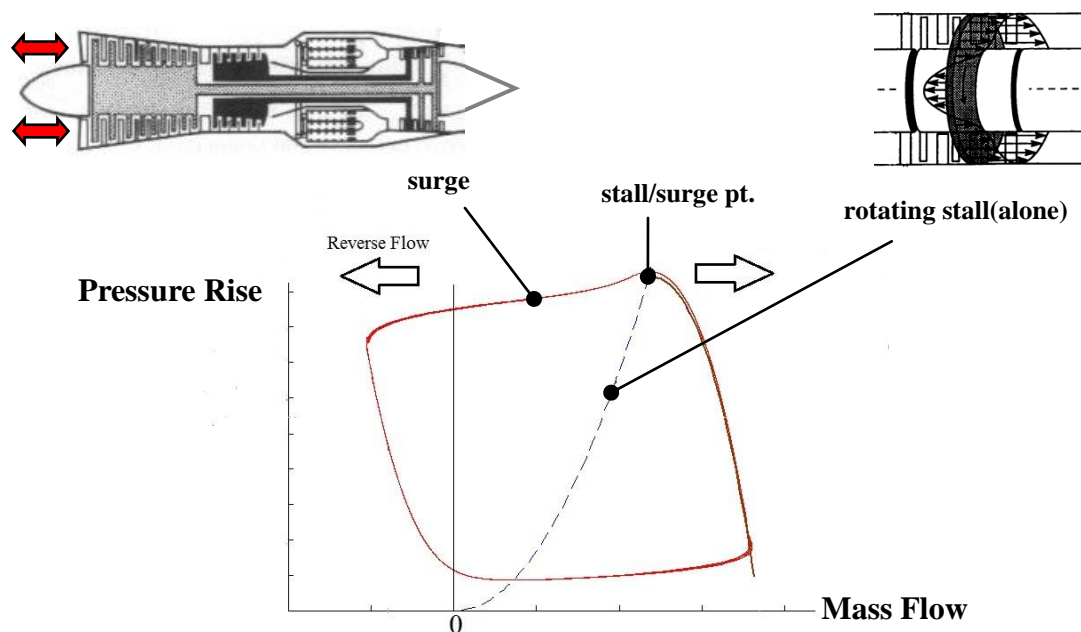


Figure 1-7: Aerodynamic instabilities for a compressor

1.3 Problem Definition

To avoid surge during engine operation, the design point of the compressor is placed away from the stall/surge point. As the engine accelerates or decelerates the compressor operates along a line called *running line* that intersects this point, as shown in Figure 1-6. The running line is set by a thermodynamic balance between the compressor combustor and turbine at the different operating speeds. For a particular gas turbine, this line can be set by the turbine design. The distance between the running line and stall/surge line is referred to as the surge margin. However, neither the surge line nor running line are fixed in an actual gas turbine engine. Engine inlet flow distortion and engine wear usually causes the surge line in Figure 1-6 to move to the right whereas rapid engine acceleration will make the running deviate to the left, both factors reducing surge margin and putting an engine at risk for surge during its operating life time. Furthermore, while the designer may try to incorporate adequate stall/surge margin, given the difficulty in accurately predicting the compressor stall point, the compressor must be mapped experimentally to find the actual surge line. Thus, it is inevitable that the gas turbine will be surged repeatedly

during its development phase. As such, one must ensure during the design phase that the components will withstand the aerodynamic load brought about by a surge event and that the gas turbine would survive the flow oscillation in conditions of the cooling flow extracted inside the compressor.

As rotating stall is usually the trigger for surge, much of research on aerodynamic instabilities over the past few decades has focused on predicting rotating stall as in the work by Day [3] and suppressing its inception [4] to extend stall/surge margin. Relatively little research has been performed on surge. Some of this research have looked at analytically simulating the surge cycle for low-speed axial compressors as a whole, such as reference [5], while others more recent work focused on CFD simulations of compressors with final 3-D blade geometries as described in [6]. However, at the preliminary design phase of an engine, the three-dimensional compressor blade geometries are not yet defined. Instead, only the gas path and blade chord, thickness and inlet/exit angles at the mean radius along the gas path (meanline) and blade count are determined through rapid iterations using analytical models that rely on quasi-1-D flow physics and loss correlations to predict the compressor map (and turbine map) and by extension the engine performance. Yet, it is based on the results from the preliminary design phase that engine weight and performance specifications and component design objectives are set for the rest of the design, making this phase extremely important. Consequently, it is important to have an idea at this phase about the aerodynamically induced forces involved during surge for proper preliminary dimensioning of engine components. An estimate of oscillation frequency would also be useful for prevent resonance of certain components. Thus, there is a need for a method to predict, right from the preliminary design phase and even with order-of-magnitude accuracy in amplitude, the oscillations of flow parameters (mainly pressure, velocity/momentum and mass flow) at relevant points inside a multi-stage compressor required for calculating aerodynamics forces and cooling bleed mass flows during surge.

1.4 Objectives

The objective of this research is to develop and evaluate a rapid method to predict, within order of magnitude accuracy or better, the temporal variation during a surge cycle of flow properties at pertinent meridional locations along the meanline of a multi-stage axial or non-axial compressor. These locations could be the compressor inlet or exit or at locations between certain blade rows

where air extractions are taken or when flow properties are needed for a control volume analysis to calculate the aerodynamic forces on a blade row or on the shaft holding multiple compressor blade rows. This method is to be used in the preliminary phase when rapid design iterations are being carried out.

1.5 Thesis Outline

Following this introduction chapter, this remainder of the thesis is organized as follows:

Chapter 2 contains a literature review covering past research on compressor surge simulations to identify pertinent works that will contribute to the method developed in this project.

Chapter 3 presents the method proposed and the way in which it is implemented numerically for surge simulations. It also describes the axial and non-axial compressor geometries that will serve as test cases to evaluate the proposed method.

Chapter 4 presents the results of the method as applied to the studied geometries along with an assessment of the effectiveness of the method with regard to the objectives of the study.

Finally, Chapter 5 summarizes the main conclusions of this study and presents suggestions for future work.

CHAPTER 2 LITERATURE REVIEW

This chapter presents an overview of the state of the art in compressor surge simulations. This information will be highly useful for developing a method for predicting surge induced flow oscillations within multi-stage compressors according to the objective of the current research. The past works in this field can be placed under two categories, namely analytical methods and computational methods.

2.1 Analytical Methods

In the 1950s, Emmons et al. [7] were the first to identify the two compressor aerodynamic instabilities, namely rotating stall and surge, through experiments on different compressors. They stipulated that a compression system is dynamically unstable near the peak of the pressure rise/mass flow characteristic (speedline) as its slope becomes positive. They proposed a qualitative explanation for rotating stall based a rotating pattern of 2-D blade suction side boundary separation and used a Helmholtz resonator analogy for surge. In the latter case, the compressor/duct length and combustor volume were modelled as the pipe length and plenum volume to get a rough estimate of the oscillation frequency.

The next significant development in surge modelling only came about two decades later when Greitzer [5] proposed a lumped-parameter model to simulate surge in low-speed (incompressible) axial compressors. Recognizing that surge involves not just the compressor but other elements of the entire compression system, Greitzer modelled the main components of a gas turbine with discrete lumped elements, namely an actuator disk as the compressor, a plenum to model the combustor and a throttle as the turbine, as illustrated in Figure 2-1. The flow is incompressible in all components except in the plenum.

The compressor is modelled as an actuator disk that incorporates fluid inertia across which the instantaneous pressure rise is given by the steady pressure rise, obtained through the speedline at the given instantaneous mass flow from which is subtracted the inertia of the fluid across the compressor (and associated duct). The combustor is modelled as a plenum volume of stagnant compressible gas with spatially uniform properties whose pressure matches the exit pressure of the compressor and inlet pressure of the turbine. The compression/expansion process in the plenum is assumed to be isentropic. Finally, the turbine is simply treated as a throttle with a

quadratic relationship between pressure drop and mass flow that dumps the air into the same reservoir pressure as that at which the air enters the compressor. Thus, the total-to-static pressure rise across the compressor is the same as the static pressure drop across the turbine.

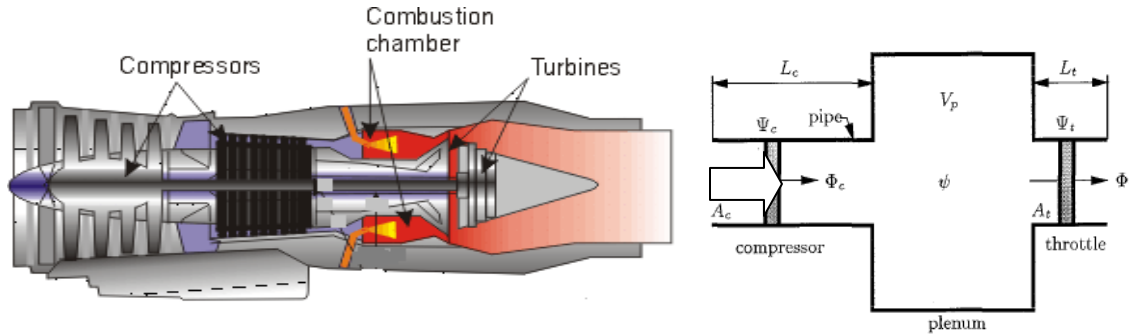


Figure 2-1: Schematic of Greitzer model [5]

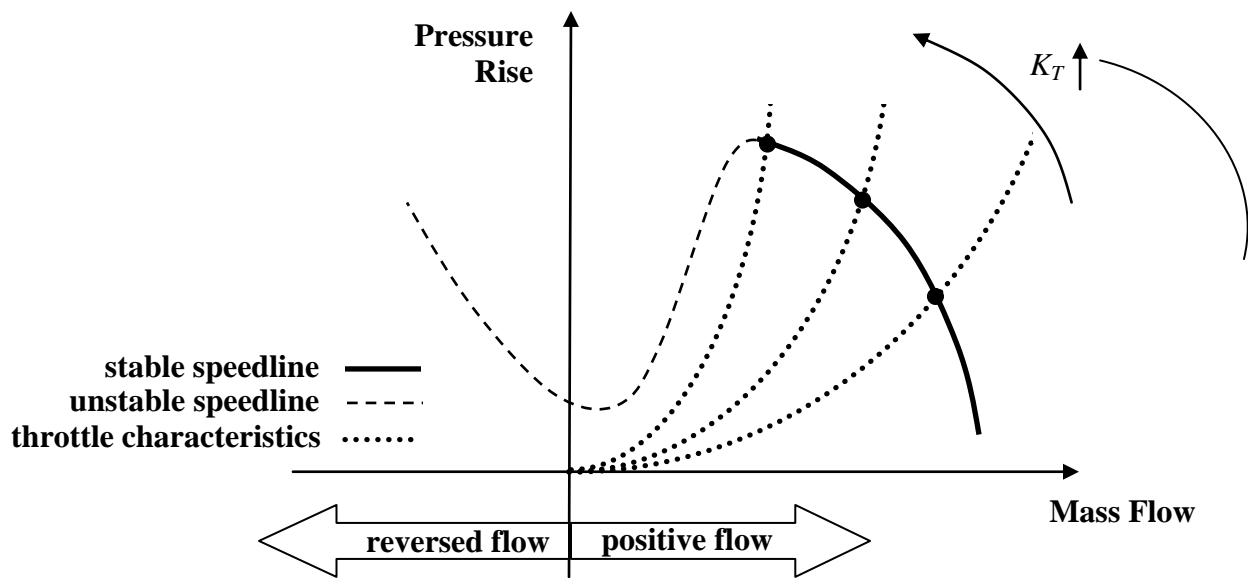


Figure 2-2: Operating points from pressure matching between compressor and throttle (turbine)

The result of the pressure matching between the three components in the Greitzer model is illustrated in Figure 2-2, which shows the compressor speedline, with the stable part being the solid line and the unstable part ('axisymmetric' stall condition) the dashed line. The throttle characteristics (pressure drop versus mass flow) are shown as dotted lines for different throttle openings, each opening described by a constant value of K_T . When the compressor is operated in the stable region, the operating point represents the intersection of the stable part of the speedline

for and the throttle characteristic, where the pressure matches for the same mass flow. As the throttle is closed (value of K_T increased), the flow settles to a new stable operating point up the speedline. However, beyond the last stable point, i.e. the stall/surge point, there is no longer an equilibrium point where pressure matches at the same mass flow across the compressor and turbine and the solution will go to a limit cycle (surge). The results from the Greitzer model compared well with experiments as shown in Figure 2-3.

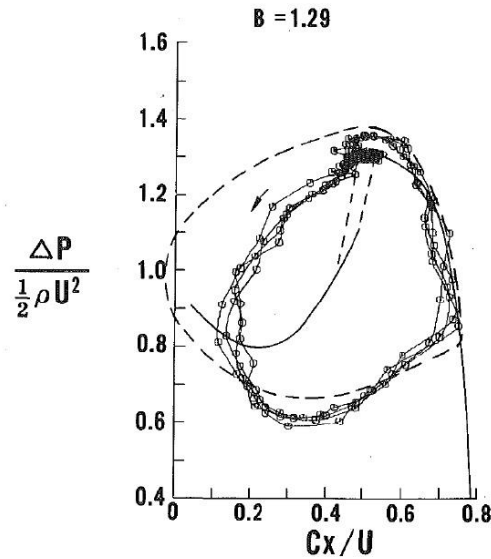


Figure 2-3: Experimental validation of model by Greitzer[8]

In addition, Greitzer also proposed a non-dimensional parameter called B-parameter, as a similitude parameter for surge behavior among different compression systems. This parameter can according to him be used to predict whether a compression system will exhibit surge or remain in rotating stall. As defined in equation (2.1) the B parameter involves the compressor rotating speed (U), sound speed (a), annular area (A), length (L) and plenum volume (V).

$$B = \frac{U}{2a_s} \sqrt{\frac{V}{AL}} \quad (2.1)$$

Based on theory and experimental data of a low-speed axial compressor with different plenum volumes, as presented in Figure 2-4, Greizer [8] showed that surge would only occur for B greater than 0.7 or 0.8. Thus an increase in plenum volume and/or rotation speed will tend to drive the system toward surge.

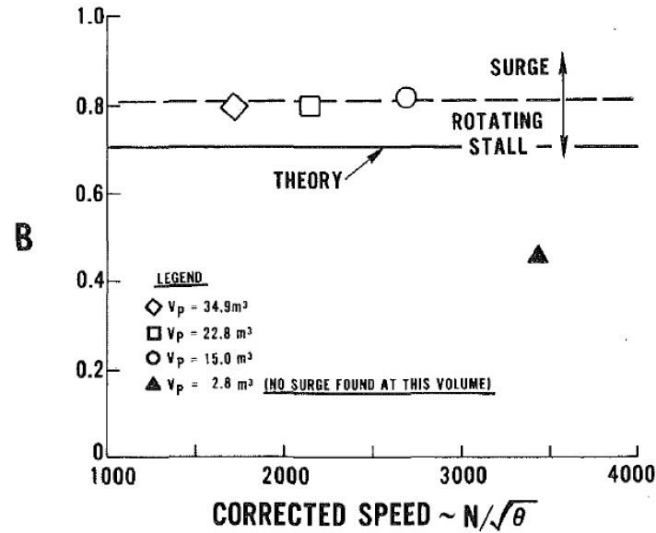


Figure 2-4: Onset of surge for different plenum volume[8]

Greitzer [8] showed two experimental cases, both presented in Figure 2-5, one with low speed and high plenum volume and the other with higher speed and lower plenum volume but with about the same value of the B parameter. One can see that the surge limit cycle is essentially the same justifying the claim of the B parameter as a similitude parameter.

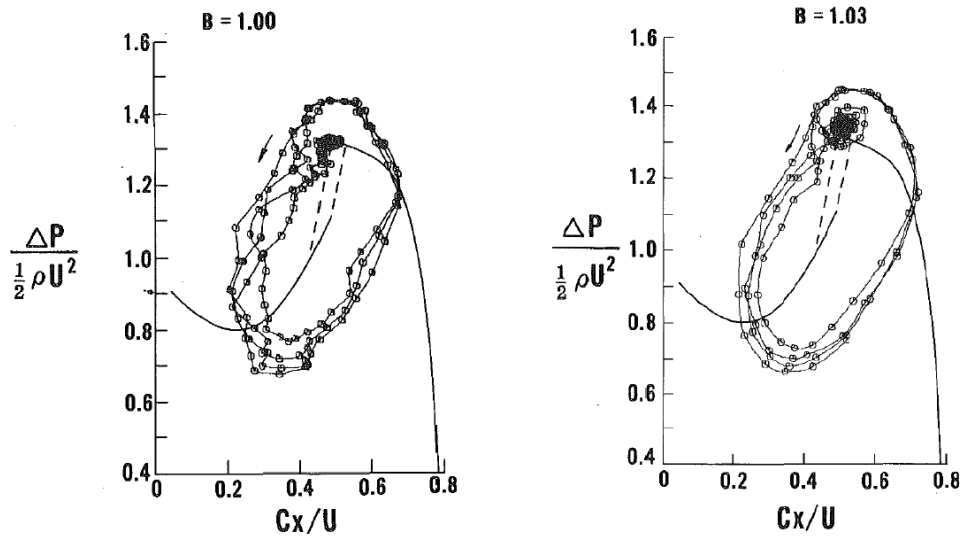


Figure 2-5: Experimental results for two surge cycle with the same B parameter [8]

The Greitzer model has the advantages of simplicity, calculation speed and the capability to provide good results. However, it has certain notable drawbacks. First, it requires not only the stable part of the speedline but also the unstable part (which includes the negative flow region) as

shown by the dashed line in Figure 2-2, which is very hard to obtain either experimentally or even computationally and certainly not known at the preliminary design phase. Second, in treating the compressor as a single actuator disk, one cannot obtain the flow parameters inside of the compressor. Third, the role of the B parameter as a similitude parameter has been questioned by subsequent work. While Greitzer [8] showed similarity of the surge limit cycle in Figure 2-5 for the same B parameter, he did not compare the temporal variation of pressure and mass flow to show whether the oscillations have the same frequency. Works by other researchers [6, 9] later showed that the surge limit cycle shape on the compressor map can be the same for the same B parameter without the oscillation frequency being the same. Last but not least, due to the assumptions of axial flow and incompressibility, the model is limited to low-speed axial compressors. However, Hansen et al [10] demonstrated experimentally that the model seems to apply also be adapted to a centrifugal compressor although without proving it analytically. However, his results also showed that the critical B parameter value of 0.8 for surge does not apply in this case. Similarly, Day [11] also showed experimentally, on a low-speed axial compressor, that this critical B parameter value is not universal.

Nevertheless, the Greitzer model formed the basis for many subsequent analytical modelling works on compressor aerodynamic instabilities, most of which concentrated on prediction and suppression (through flow control) of rotating stall inception. These works started with those by Moore[12] and Moore and Greitzer [13, 14] who expanded lumped-parameter model to include the circumferential flow variation in order to capture rotating stall in low-speed axial compressors. Bonnaure [15] developed a two-dimensional compressible model in the axial multi-stages compression system that relied on loss and deviation correlations for each blade row. The model is used to predict the onset of stall but does not predict the surge cycle. Spakovszky [16] developed a new model to predict the radial effects on the compression system, but this model is suitable for control purposes and cannot be developed to predict the surge cycle. Weigl [17] introduced another model developed from the Bonnaure [15] work, but which was also used for rotating stall inception.

More recently, Morini et al. [18] proposed a model based on a modular approach in which each component (inlet or exit plenum, duct, compressor) can be discretized into multiple elements instead of one lumped parameter and the one-dimensional equations of conservation of mass, momentum and energy equations can be solved using the finite difference method. In principle,

this modular approach should allow for putting together complex combinations of the elements of a compression system and even include heat transfer through the energy equation. However, the authors only solved for a standard volume-duct-compressor-duct-volume combination in which the compressor seems to have been treated in one lumped-parameter approach through the speedline as with the Greitzer model. Their placement of the emphasis on solving the equations in the ducts is not really relevant in an aero-engine where un-bladed ducts are kept to a minimum.

2.2 Computational Methods

The computational methods for surge simulations can be divided into two types, quasi-1D and 3D CFD. The quasi-1D computational methods started with the DYNTECC model of the compression system by Hale and Davis [19]. This model consists of discretizing the entire gas path of the compression system into elemental control volumes across which the 1-D conservation equations are applied along with source terms to account for the effects of blade forces, shaft work, mass bleed and heat transfer. These source terms must be determined from a complete set of stage pressure rise and temperature rise characteristics. The conservation equations are then solved through a finite difference numerical technique. Cousins [20] applied the DYNTECC model to simulate surge in an axial-centrifugal compressor. Garrard [21] later extended the DYNTECC model by incorporating modelling of the combustor and turbine to produce the ATEC model that can simulate the entire gas turbine. More recently, Du and Leonard [9] applied a similar method as the DYNTECC model in which the gas path of a compression system is discretized and the adapted 1D Euler equations are applied with source terms estimated from calculating the velocity triangles for each blade row and loss and blade deviation correlations. The 1D approaches above give good results in terms of simulating the surge cycle and would allow for the extraction of flow information inside the compressor during surge. However, they involve some preparation work in extracting the source terms and in obtaining a mesh independent solution.

With the increase in computational capabilities in recent years, a full 3-D computational approach has been proposed by several researchers. Niazi [22] simulated surge in an axial compressor with CFD using an unsteady RANS CFD research code. A full-annulus isolated compressor rotor was meshed and the effect of the downstream components was simulated through a dynamic boundary condition applied at the exit of the computational domain that gives the variation of the

pressure inside a plenum through an analytical equation. However, the turbine was not properly modelled in this equation as a simple constant mass flow rate was imposed at the plenum exit. The predicted temporal variations of pressure rise and flow coefficient are qualitatively reasonable but somewhat noisy. However, the results remain questionable due to the non-physical constant exit mass flow condition for the plenum.

Guo et al. [23] later applied the approach of Niazi [22] to simulate surge for an impeller using the RANS model of the commercial CFD code ANSYS CFX. In doing so, they used the same constant exit mass flow condition for the plenum model. Some of their results were highly irregular with non-repeatable surge cycles.

Vahadati et al. [24] carried out CFD simulations of surge in an eight-stage axial compressor by meshing only one blade passage per blade row. Instead of a plenum and valve, they included a meshed converging nozzle in the computational domain downstream of the compressor. The use of only one blade row per blade passage is an ingenious way of taking advantage of the essentially one-dimensional nature of surge while reducing computational requirements. However, the drawbacks of this work are the need to modify the nozzle shaped and remesh for each simulated point up the speedline in search for the stall/surge point and the challenge in correctly representing combustor and turbine properties with the nozzle on a quantitative basis.

Finally, Dumas [6] combined the best features of the above approaches in a method for simulating surge in any multi-stage compressor. As illustrated in Figure 2-6, his approach essentially consists of using single blade passage multi-stage RANS CFD simulations of the compressor with ANSYS CFX, as done by Vahadati et al. [24], but for which a dynamic exit boundary conditions was applied at the compressor computational domain exit, similar to the strategy proposed by Niazi [22]. However, unlike Niazi [22], to analytical equation for the dynamic exit boundary condition was obtained using the same modelling approach as Greitzer in which the turbine was represented as a valve with a quadratic pressure-mass flow relationship rather than a constant mass flow condition. This method was used to simulate surge on three compressor geometries: a low-speed three-stage axial compressor for which surge data exists; a low-speed axial-centrifugal compressor with small compressibility effects composed of the previous three-stage axial compressor matched to an impeller with a vaneless diffuser; and a high-speed mixed-flow-centrifugal compressor in which the compressibility effects are

important. In spite of very limited test data for validation, Dumas [6] showed that the simulations worked well though a good match with the measured surge cycle for the low-speed three-stage axial compressor as shown in Figure 2-7.

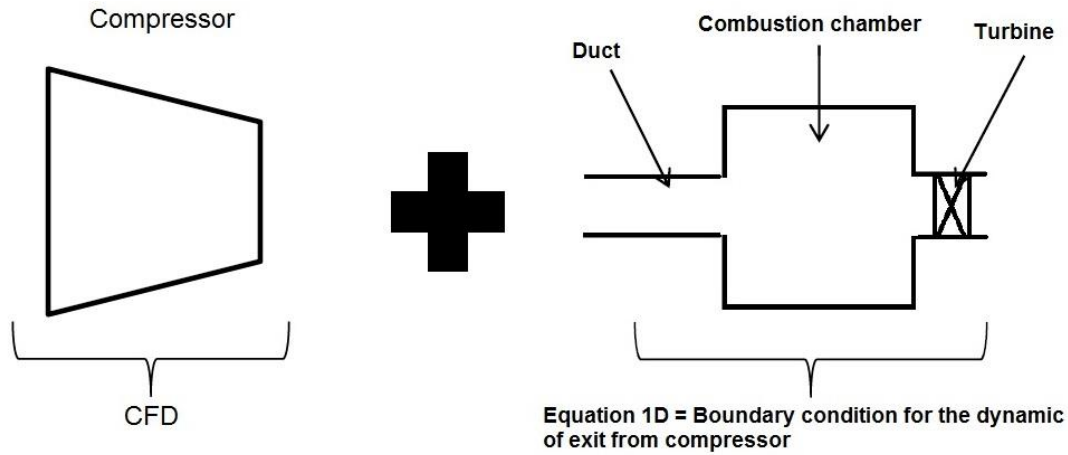


Figure 2-6: Illustration of the methodology used by Dumas [6]

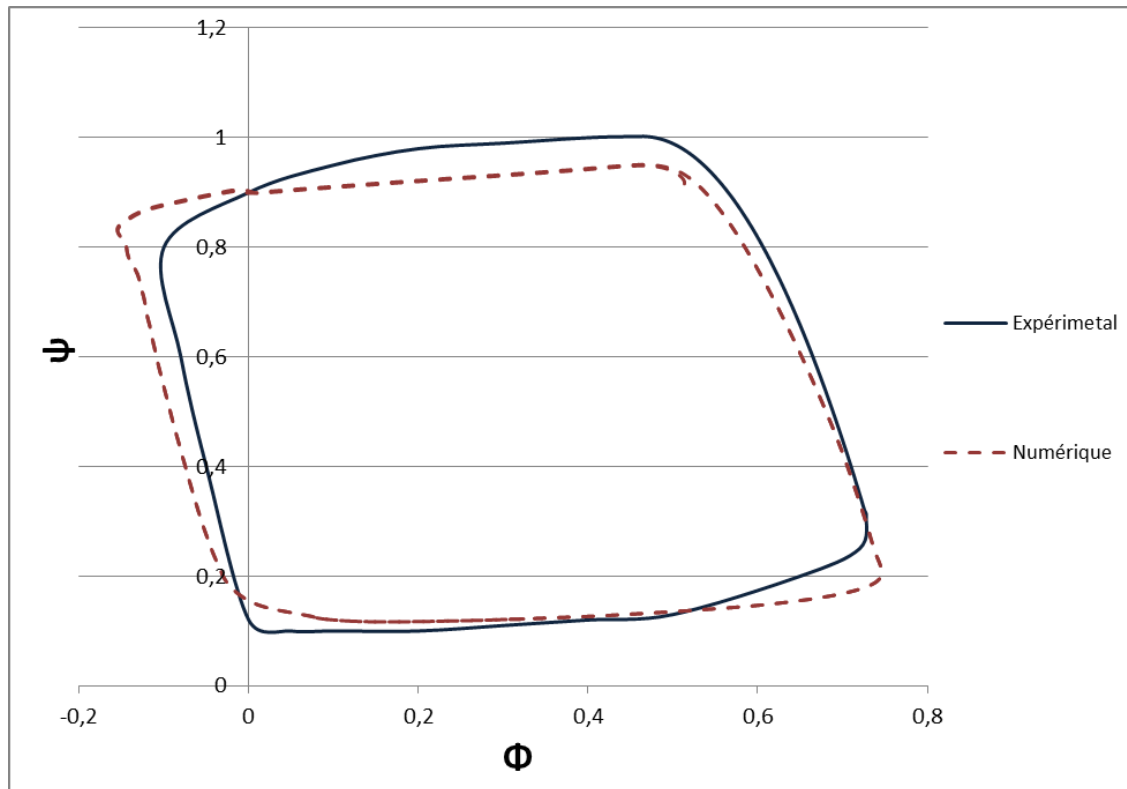


Figure 2-7: Comparison of simulated surge cycle of low-speed axial compressor by Dumas with test data[6]

The full 3D RANS CFD approach, culminating in the work by Dumas [6], can deliver all local flow information at any point inside the compressor during surge to a greater extent than any approach so far without requiring any empiricism beyond the turbulence models and numerical issues associated with CFD simulations. However, this approach requires knowledge of the three-dimensional blade geometries, preparation work on mesh dependency studies, as well as relatively significant computational resources and time.

CHAPTER 3 METHODOLOGY

This chapter describes the methodology taken to address the objectives of this project starting with a qualitative description of the general strategy, followed by the setup of equations and verification of applicability to non-axial compressors. The chapter concludes with a description of three compressor geometries to be used for evaluation of the model and the procedure for running the model.

3.1 General Strategy

Chapter 2 provided an overview of the different strategies taken in the past to simulate surge, ranging from analytical models to full-scale 3D RANS CFD simulations. The objective of this project is to provide a fast method to predict, within order of magnitude accuracy or better, the temporal variation of flow properties at relevant location in a multi-stage compressor during surge, to be used during the preliminary design stage. Consequently, the 3-D RANS CFD approach cannot be considered, not only because it is time-consuming, but also because the full blade geometries are not available at the early design stage. Among lower-fidelity models, the quasi-1D models would be a good option; however, they do require work for extracting source terms from the compressor characteristics and for discretizing the compression domain, which is not ideal at the preliminary design phase where there is a need for rapid turn-around time during preliminary design iterations. As a result the strategy chosen was to develop a method based on the Greitzer model, but with the addition of a new element to allow for extracting flow property variations at points of interest inside the compressor.

The proposed strategy consists of using the Greitzer model approach to predict the surge cycle of the entire compressor and then deduct from the compressor exit pressure the unsteady pressure rise associated with the compressor section between the desired location and the compressor exit. The unsteady pressure rise of the last section would comprise the steady pressure rise and the fluid inertia effects associated with this section. With the incompressibility assumption in the Greitzer model, the flow oscillation at the desired section can be simply deduced from the local cross flow area and mass flow conservation. This strategy is illustrated in Figure 3-1 for a three stage compressor in which the inquiry plane lies between the second and third stage. This is essentially the new contribution of this work.

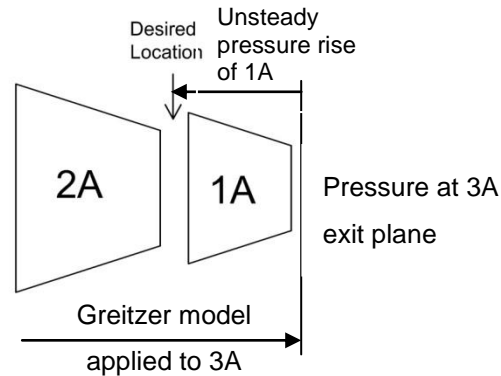


Figure 3-1: Example of proposed surge simulation strategy applied to a three-stage axial compressor

The advantage of this method is that it is simple and very fast, not only in run calculation time but also in preparation time since it would directly use the speedline (for the whole compressor and relevant sections) output from the meanline code at the preliminary design stage without any need to extract source terms, nor loss/deviation correlations that are implicit in the meanline code. However, the Greitzer approach presents two drawbacks for applications to generic multi-stage compressor. First, it was meant only for axial compressors. Nevertheless, Hansen et al. [10] did suggest, through comparison with experimental data, that the model can be applied to a centrifugal compressor and this will be verified analytically. Second, the model assumes incompressible flow inside the compressor. However, compressibility would reduce the amplitude of pressure oscillations through absorption of some of the energy in compression of the fluid. As such the incompressible model with air density taken at the inlet value should provide a conservative estimate of pressure oscillation amplitudes that may be adequate for an order-of-magnitude prediction accuracy requirement, which can be assessed through case studies.

While the Greitzer approach is chosen, the improved version of the model called the Moore-Greitzer model as described by Moore and Greitzer [13] is chosen as the surge simulation strategy for the entire compressor. This model adds the circumferential dimension to the Greitzer model enabling it to predict both surge and rotating stall. While rotating stall is not the focus of the present work, the Moore-Greitzer formulation provides more adequate and detailed representation of the compressor blade rows in the calculation of the inertia effects, which is

important in this case to extract flow information within the compressor. At the same time, it also gives the final method the potential capability of simulating rotating stall.

3.2 Model Formulation

The equations of the Moore-Greitzer [13] model are derived for the basic compression configuration laid out in Figure 3-2, which is composed of an inlet duct of length (L_I), a multi-stage compressor, an exit duct of length (L_E), a plenum and a throttle valve. With the exception of the plenum, the flow in the rest of the system is treated as incompressible. It is assumed that the two ducts are lossless and that the turbine dumps air into an exit static pressure equal to the total pressure of the air entering the compressor. This is usually the case for a gas turbine engine where the exhaust static pressure and inlet total pressure are at the value of the atmospheric pressure.

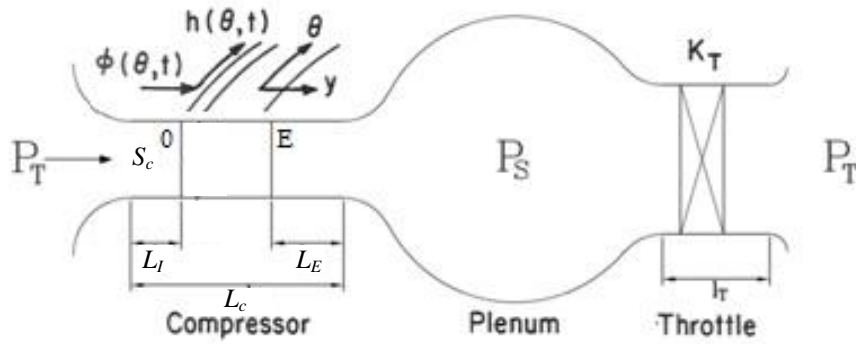


Figure 3-2: Schematic of compression system[13]

3.2.1 Compressor and Ducts

The instantaneous total-to-static pressure rise ($P_{out} - P_{T,in}$) across the duct-compressor-duct system can be taken as the steady-state total-to-static pressure rise across the compressor ($P_{out} - P_{T,in}$)_{ss} minus the static pressure drop associated with the inertia effect $\Delta P_{inertia}$ from acceleration of the fluid in the ducts and compressor blade passages as shown in equation (3.1).

$$P_{out} - P_{T,in} = (P_{out} - P_{T,in})_{ss} - \Delta P_{inertia} \quad (3.1)$$

The inertia term can be calculated by considering the approximate blade geometries and duct lengths and knowing from the unsteady Bernoulli's equation that the static pressure difference

due to unsteadiness between two points along a streamline is given by $\rho L(dv_s/dt)$, where ρ , L and (dv_s/dt) are the respectively, the density, streamline length and time rate of change of streamwise velocity in the relative frame. As such, for a turbomachinery blade passage with a blade chord b and stagger angle γ and a meridional velocity C_m as illustrated in Figure 3-3, the unsteady pressure drop due to inertia effect are given by equations (3.2) and (3.3) for a stator and a rotor, respectively. The multiplier k is a correction factor for b to account for the distances between blade rows and curvature effects to blade passage curvature (the latter neglected in this study). In the case of the rotor, U is the circumferential rotational speed at the compressor inlet mean radius. In a similar manner, equation (3.4) gives the inertia effect for a duct with duct length L_{duct} in which the flow has a swirl angle α (which is usually zero as for the cases studied in this work).

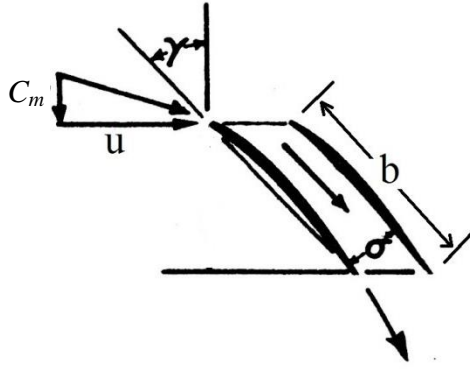


Figure 3-3: Blade passage approximation for calculating inertia effect

$$\Delta P_{inertia, stator} = \rho k b \frac{D(C_m / \cos \gamma)}{Dt} = \frac{\rho k b}{\cos \gamma} \frac{\partial C_m}{\partial t} \quad (3.2)$$

$$\Delta P_{inertia, rotor} = \rho k b \frac{D(C_m / \cos \gamma)}{Dt} = \frac{\rho k b}{\cos \gamma} \left(\frac{\partial C_m}{\partial t} + \frac{\partial C_m}{\partial \theta} \frac{d\theta_{rotor}}{dt} \right) = \frac{\rho k b}{\cos \gamma} \left(\frac{\partial C_m}{\partial t} + \frac{\partial C_m}{\partial \theta} \frac{U}{R} \right) \quad (3.3)$$

$$\Delta P_{inertia, duct} = \rho L_{duct} \frac{D(C_m / \cos \alpha)}{Dt} = \frac{\rho L_{duct}}{\cos \alpha} \frac{\partial C_m}{\partial t} \quad (3.4)$$

Incorporating equations (3.2) through (3.4) for all blades rows and ducts into equation (3.1) gives equation (3.5).

$$P_{out} - P_{t,in} = (P_{out} - P_{t,in})_{ss} - \left[\sum_1^{N_{rotor}} \frac{\rho k b}{\cos \gamma} - \sum_1^{N_{stator}} \frac{\rho k b}{\cos \gamma} - \sum_1^{N_{ducts}} \frac{\rho L_{duct}}{\cos \alpha} \right] \frac{\partial C_m}{\partial t} - \left[\sum_1^{N_{rotor}} \frac{\rho k b}{\cos \gamma} \right] \frac{\partial C_m}{\partial \theta} \frac{U}{R} \quad (3.5)$$

Non-dimensionalizing equation (3.5) with the four non-dimensional parameters defined below and assuming zero swirl in the inlet and exit ducts ($\alpha=0$) gives equation (3.6), in which $\Psi_c(\varphi)$ is the steady-state axisymmetric total-to-static compressor pressure rise characteristic (speedline).

1. $\varphi \equiv \frac{C_m}{U}$ Dimensionless mass flow coefficient
2. $\Psi \equiv \frac{P_{out}-P_{T,in}}{\rho U^2}$ Dimensionless total-to-static pressure-rise coefficient
3. $l \equiv \frac{L}{R}$ Dimensionless length
4. $\xi \equiv U \frac{t}{R}$ Dimensionless time

$$\Psi = \Psi_c(\varphi) - (l_I + l_R + l_S + l_E) \frac{\partial \varphi}{\partial \xi} - l_R \frac{\partial \varphi}{\partial \theta} \quad (3.6)$$

, where $l_R \equiv \sum_1^{Nrotor} \frac{kb}{R \cos \gamma}$; $l_S \equiv \sum_1^{Nstator} \frac{kb}{R \cos \gamma}$; $l_I \equiv \frac{L_I}{R}$; $l_E \equiv \frac{L_E}{R}$

Next, to introduce the circumferential perturbation associated with rotating stall, as detailed in Moore and Greitzer [13] and summarized here, the flow coefficient φ is split into an axisymmetric part Φ that accounts for steady-state operation plus axisymmetric (surge-type) perturbations and a circumferentially varying part g (meridional direction) and h (circumferential direction) for rotating stall-type perturbations, as shown in equation (3.7), where g and h integrate to zero over the circumference and can be obtained from a perturbation potential $\tilde{\phi}'(\xi, \eta, \theta)$ evaluated at the compressor inlet (station 0 in Figure 3-1). This potential exists through an irrotational flow assumption for the upstream duct. The variable η is the axial distance, non-dimensionalized by R , with the origin at station 0.

$$\varphi(\xi, \theta) = \Phi(\xi) + g(\xi, \theta); (\xi, \theta) = (\tilde{\phi}'_{\eta})_0; h(\xi, \theta) = (\tilde{\phi}'_{\theta})_0 \quad (3.7)$$

Incorporating equation (3.7) into (3.6) and given that the perturbations g and h apply only to the compressor, one obtains equation (3.8). The term $m(\tilde{\phi}'_{\xi})_0$ accounts for pressure perturbations in the exit duct in which the flow is assumed rotational with very small pressure perturbations. The value of m is 1 for a short exit duct and 2 for a long exit duct.

$$\Psi = \Psi_c \left(\Phi + (\tilde{\phi}'_{\eta})_0 \right) - (l_I + l_R + l_S + l_E) \frac{d\Phi}{d\xi} - m(\tilde{\phi}'_{\xi})_0 - l_R(\tilde{\phi}'_{\xi\eta} + \tilde{\phi}'_{\theta\eta})_0 - l_S(\tilde{\phi}'_{\xi\eta})_0 \quad (3.8)$$

To remove the derivative in η Moore and Greitzer [13] introduced a simplification based the fact that the perturbation g is circumferentially periodic, and keeping only the first term of the Fourier series solution for $\tilde{\phi}'_{\eta\eta} + \tilde{\phi}'_{\theta\theta} = 0$ which results in $(\tilde{\phi}'_{\eta})_0 = -(\tilde{\phi}'_{\theta\theta})_0$ allowing one to define a perturbation function $Y(\xi, \theta) \equiv (\tilde{\phi}')_0$ which gives $(\tilde{\phi}'_{\eta})_0 = -Y_{\theta\theta}$. Thus, equation (3.8) becomes:

$$\Psi = \Psi_c(\Phi - Y_{\theta\theta}) - (l_I + l_R + l_S + l_E) \frac{d\Phi}{d\xi} - mY_{\xi} + l_R(Y_{\xi\theta\theta} + Y_{\theta\theta\theta}) + l_S Y_{\xi\theta\theta} \quad (3.9)$$

Finally, the inertia terms for the blade rows are combined through the definition of an average inertia parameter τ defined as in equation (3.10) which allows for the combination of the terms l_R and l_S into a single term $1/a$ where a is defined as in equation (3.11) so that equations (3.9) simplifies to equation (3.12).

$$\tau \equiv \frac{2(l_R + l_S)R}{UN_{stages}} \quad (3.10)$$

$$a \equiv \frac{R}{U\tau N_{stages}} \quad (3.11)$$

$$\Psi(\xi) = \Psi_c(\Phi(\xi) - Y_{\theta\theta}) - l_c \frac{d\Phi}{d\xi} - mY_{\xi} + \frac{1}{2a}(2Y_{\xi\theta\theta} + Y_{\theta\theta\theta}) \quad (3.12)$$

, where $l_c \equiv l_I + \frac{1}{a} + l_E$

The last equation which gives the pressure rise from the gas turbine engine inlet to the end of the stator of the plenum is obtained by integrating the equation (3.12) over the circumference, considering that $\int_0^{2\pi} Y(\xi, \theta) d\theta = 0$, which results in equation (3.13)

$$\Psi(\xi) = \frac{1}{2\pi} \int_0^{2\pi} \psi_c(\Phi(\xi) - Y_{\theta\theta}) d\theta - l_c \frac{d\Phi}{d\xi} \quad (3.13)$$

The fine details of the above derivations and of the definitions of the different parameters used can be found in references [12, 13].

3.2.2 Plenum and Throttle

From the lumped parameter approach of Greitzer, the air in the plenum is assumed to be an ideal gas at rest with spatially uniform properties as illustrated in Figure 3-4. The compression/expansion process in the plenum is assumed to be isentropic.

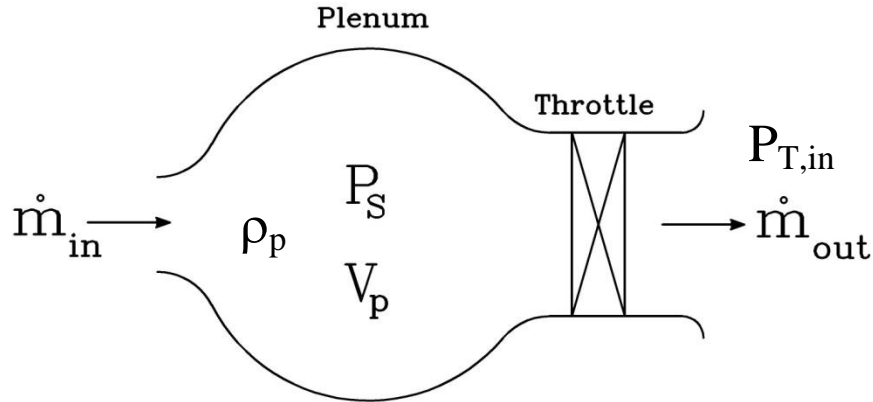


Figure 3-4 : Modelling of plenum and throttle

Mass conservation (\dot{m}) applied to the plenum results in equation (3.14)

$$\dot{m}_{in} - \dot{m}_{out} = \frac{d(\rho_p V_p)}{dt} = V_p \frac{d(\rho_p)}{dt} \quad (3.14)$$

With the ideal gas law $P = \rho \tilde{R}T$, where $\tilde{R} = 287 \text{ J} \cdot \text{Kg}^{-1} \cdot \text{K}^{-1}$ is the specific gas constant for air and an isentropic process $P^{1-\gamma} T^\gamma = \text{Constant}$, where γ is the specific heat ratio, one obtains equation (3.15), where a_s is the speed of sound in air. Combining equations (3.14) and (3.15) results in equation (3.16) which describes the time variation of the plenum pressure P_S with respect to the mass flow at its inlet and outlet.

$$\frac{d(\rho_p)}{dt} = \frac{1}{\tilde{R}\gamma T_p} \frac{dP_S}{dt} = \frac{1}{a_s^2} \frac{dP_S}{dt} \quad (3.15)$$

$$\frac{dP_S}{dt} = \frac{a_s^2}{V_p} (\dot{m}_{in} - \dot{m}_{out}) \quad (3.16)$$

Considering that P_S is the same as the pressure exiting the downstream duct of the compressor, that $\dot{m}_{in} = \dot{m}_{compressor} = \rho C_m S_c$, where S_c is the compressor cross-sectional area and that the

pressure drop across the throttle follows the quadratic relation laid out in equation (3.17), equation (3.16) reduces to its non-dimensional form to equation (3.18),

$$\Delta P_{throttle} = \frac{1}{2} K_t \dot{m}_{out}^2 = P_S - P_{T,in} \quad (3.17)$$

$$\frac{\partial \Psi}{\partial \xi} = \frac{1}{4B^2 l_c} \left(\Phi(\xi) - \sqrt{\frac{2\Psi(\xi)}{K_t}} \right) \quad (3.18)$$

, where $B = \frac{U}{2*a_s} \sqrt{\frac{V_p}{S_c*L_c}}$ is the Greitzer B parameter with Ψ and Φ being, respectively, the instantaneous total-to-static pressure rise coefficient and flow coefficient of the compressor-ducts system from equation (3.13).

3.2.3 Surge Simulation

Equations (3.12), (3.13) and (3.18) describe the non-linear behavior of the system for aerodynamic instabilities. In this case they were solved for the surge cycle of the entire compressor using the Galerkin procedure and MATLAB-Simulink according to the method described in Appendix A.

The model setup requires the use of a polynomial approximation for the full speedline. The format used by Moore and Greitzer [13] is a cubic polynomial described by equation (3.19), where the ψ_{c0} , H, and W parameters are shown in Figure 3-5. It is noted that the local flow coefficient in equation 3.19, $\varphi = (\Phi - Y_{\theta\theta})$, includes the term $-Y_{\theta\theta}$.

$$\Psi_c(\varphi) = \Psi_{c0} + H \left[1 + \frac{3}{2} \left(\frac{\varphi}{W} - 1 \right) - \frac{1}{2} \left(\frac{\varphi}{W} - 1 \right)^3 \right] \quad (3.19)$$

This cubic polynomial was chosen by Moore and Greitzer [13] based on the works by Koff [25, 26], which found this format to best match the full measured speedline in a low-speed multi-stage axial compressor. In the absence of a better alternative, this cubic speedline model is chosen for this study whose simulations will provide indications of the applicability of the speedline format to other compressors, in particular when unstable part of the characteristic is not known.

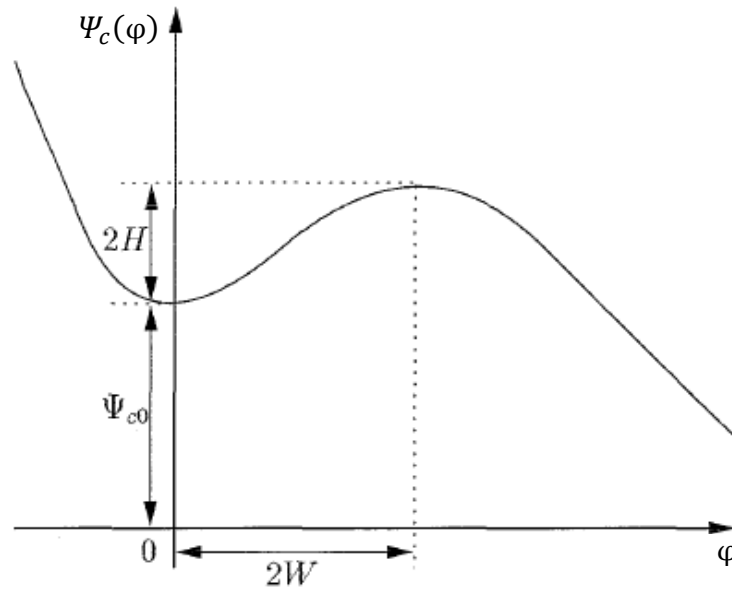


Figure 3-5: Notation used in definition of (axisymmetric) compressor characteristics

3.2.4 Surge Information Inside the Compressor

To obtain the pressure oscillation at a point between two blade rows inside a compressor such as shown in Figure 3-6, the static to static pressure rise $\psi_{SS-section2}$ and inertia effects $\Delta P_{inertia, section2}$ are simply deducted from the pressure rise $\Psi(\xi)$ and flow coefficient $\Phi(\xi)$ for the entire compressor (solved using the procedure described in Section 3.2.3 and Appendix A), as shown in equation (3.20).

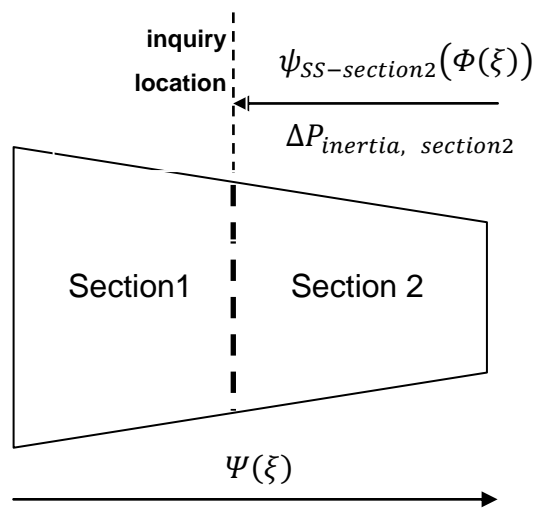


Figure 3-6: Calculation of pressure at inquiry location inside compressor

$$\Psi(\xi)_{\text{Desired location}} = \Psi(\xi) - \psi_{SS, \text{section2}}(\Phi(\xi)) + \Delta P_{\text{inertia, section2}} \quad (3.20)$$

The static pressure rise characteristic $\psi_{SS-\text{section2}}$ can easily be produced by the meanline code used during the preliminary aero-engine design phase and the inertia effect for section 2 can be calculated as in equations (3.2) through (3.4) for the blade rows and ducts located in section 2. This calculation was simply carried out in MS Excel.

It is noted that the incompressible flow assumption through the compressor means that the flow oscillations inside the compressor are in phase with that of the entire compressor. However, this may not be far from the actual surge physics. Indeed, the time scale associated with the low-frequency surge oscillation is much longer than the acoustic traveling time across the compressor. Thus, the flow fluctuations associated with surge at different points inside the compressor would essentially be in phase.

3.3 Analytical Model Assessment for Non-Axial Compressors

While the experimental assessment of the Greitzer surge model by Hansen et al. [17] suggested that this approach should work also for a non-axial compressor, it would be interesting to prove it analytically. The main element of this approach is the inertia effect. Let's consider the static pressure rise of flow through a centrifugal compressor impeller as illustrated in Figure 3-7. The Euler equation in the relative (rotating) frame, which includes a centrifugal and a coriolis terms to account for the pseudo-forces due to rotational speed Ω , is given in vector form by equation (3.21) and along the relative streamline by equation (3.22), with w and \vec{W} being the relative velocity magnitude and vector, respectively. Integrating equation (3.22) along a relative streamline going from station 1 ($l=0$) to station 2 ($l=L$) located at a higher radius results in equation (3.23), which gives the instantaneous pressure difference between the two stations.

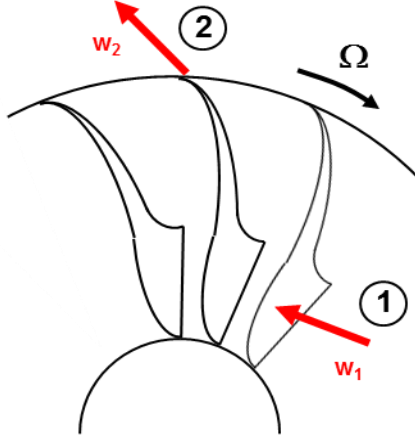


Figure 3-7: Velocity triangle at the impeller tip

$$\rho \frac{D\vec{w}}{Dt} = -\frac{1}{2} \nabla \left(p - \frac{1}{2} \rho \Omega^2 r^2 \right) - 2 \vec{\Omega} \times \vec{w} \quad (3.21)$$

$$\rho \frac{\partial w}{\partial t} + \rho w \frac{\partial w}{\partial l} = -\frac{dp}{dl} + \Omega^2 r \frac{dr}{dl} - 2\rho \vec{\Omega} \times \vec{w} \quad (3.22)$$

$$P_2 - P_1 = \frac{1}{2} \rho (w_1^2 - w_2^2) - \frac{1}{2} \Omega^2 (r_1^2 - r_2^2) - 2\rho \int_0^L \vec{\Omega} \times \vec{w} dl - \rho \int_0^L \frac{\partial w}{\partial t} dl \quad (3.23)$$

Equation (3.23) shows that the inertial effect term ($\int_0^L \frac{\partial w}{\partial t} dl$), which represents the central effect of unsteadiness through the compressor in the Greitzer modelling approach, is independent of radius change, and is thus no different than for an axial rotor. This means that the Greitzer surge model should work in non-axial geometries with non-negligible radius change.

3.4 Compressor Geometries for Model Assessment

As test data for surge are rare, the proposed surge simulation technique was assessed with the three compressor geometries used by Dumas [6] to allow assessment versus CFD data, when test data are not available. The first is a low-speed (incompressible) three stage axial geometry for which some test data are available as well as interstage data from Dumas' CFD simulations. The second compressor is a low-speed axial-centrifugal geometry, with very little compressibility effect. The last geometry is a high-speed industrial compressor composed of a mixed flow stage, and a centrifugal stage, where compressibility effects are important.

3.4.1 Low-Speed Axial Compressor

The first study focuses on a three-stage low-speed axial compressor in a rig located at the Massachusetts Institute of Technology Gas Turbine Laboratory (MIT-GTL), henceforth referred to as the MIT-GTL LS3 compressor. It incorporates an IGV (Inlet Guide Vanes) placed upstream of the first rotor. Figure 3.8 taken from Gamache [27] provide an overview of the position and shape of the blade rows and main instrumentation layout. The hub and shroud diameters are constant at 536 and 610 mm, respectively. The compressor has a nominal length of 0.67 m, while the lengths of the inlet and exit ducts are 0.86 m and 0.44 m, respectively, giving a total length (L_c) of 1.97 m. The compressor rig was adapted by Protz [28] to study surge and its suppression via active control. As illustrated in Figure 3-8, the compressor dumps air into a large plenum of 9.66 m³ in volume (to provide for a B parameter of 1), at the exit of which is a throttle valve. Downstream of this valve is a large duct that contains flow straighteners and an orifice plate for mass flow measurements as well as an exhaust fan. This fan had been used to force air in the reversed direction to obtain the reverse flow pressure rise characteristics of in the compressor [29]. This fan, however, was not operational during the surge experiments conducted by Protz[28].

The surge experiments by Protz [28] were carried out at 2600 rpm, giving a mean circumferential velocity (U) of 78 m/s. The measured surge cycle is shown in Figure 3-10 (data for B=1.02).

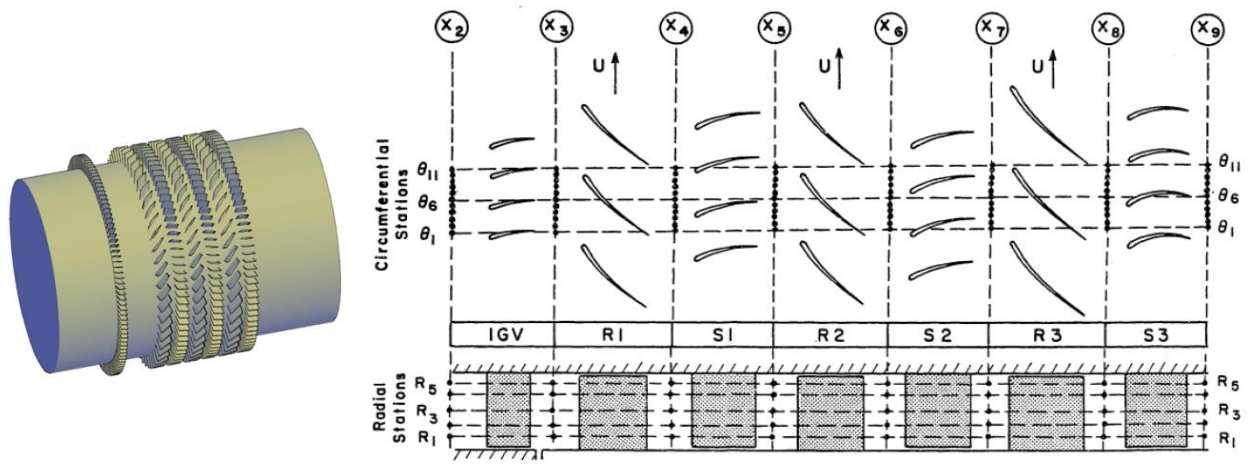


Figure 3-8: Schematic representation of the positions of the compressor blades and measurements of points for the MIT-GTL LS3 compressor [27]

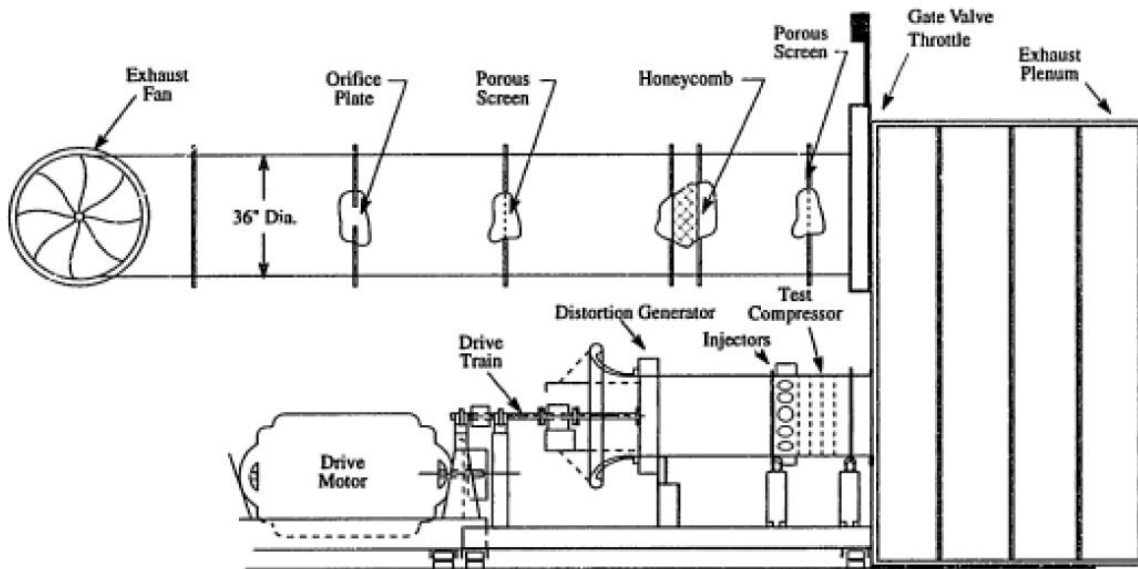


Figure 3-9 : Overview compressor MIT-GTL LS3 compressor [28]

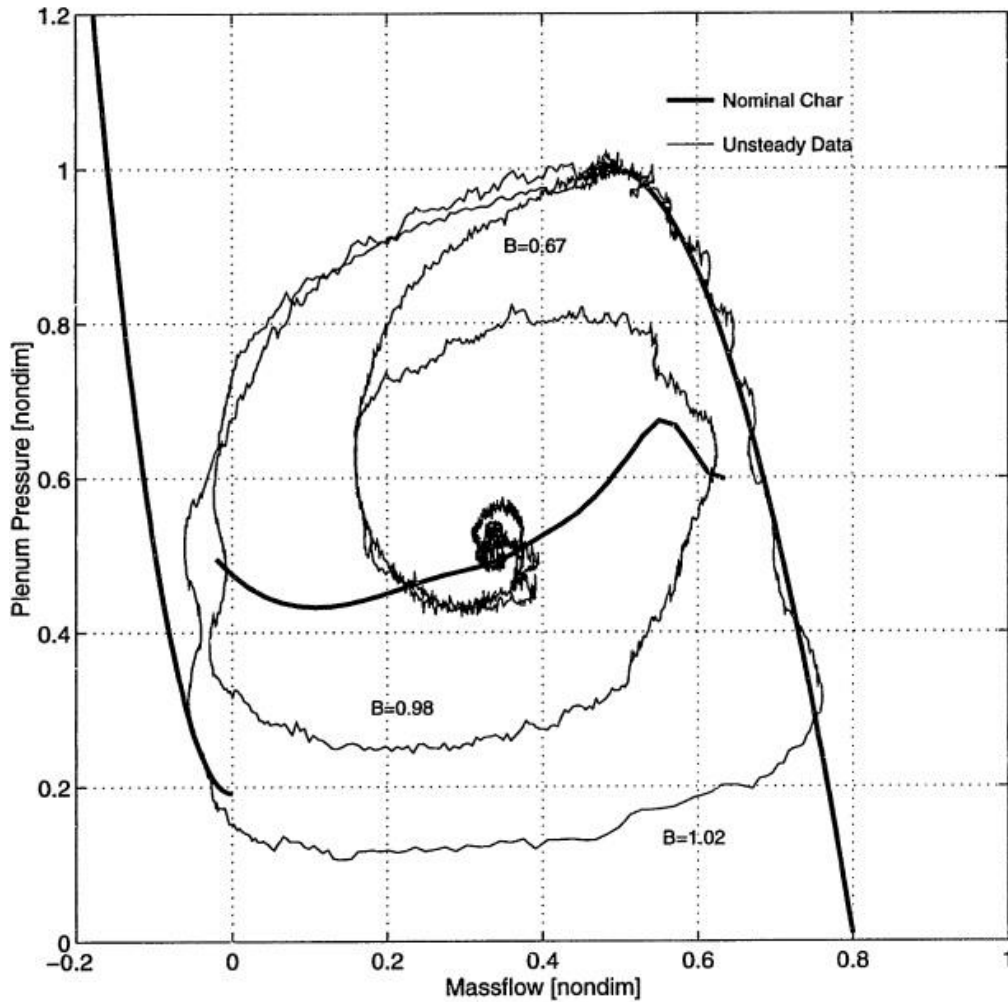


Figure 3-10: Surge cycle captured by Protz for the MIT GTL LS3 [28]

The meanline blade geometries and inter-stage distances were obtained from published works on this compressor [27, 28, 30] and the resulting modelled blade rows and dimensions used for the surge simulation modelling is illustrated in Figure 3-11. The inlet flow conditions were taken as standard atmospheric conditions. The resulting quantitative parameters used in the model is given in Table 3.1. The details of the calculation of the inertia parameter τ for this compressor and the next compressor are provided in Appendix B. This compressor has surge test data for the compressor as a whole and CFD data for pressure oscillations between the second and third stage from Dumas [6].

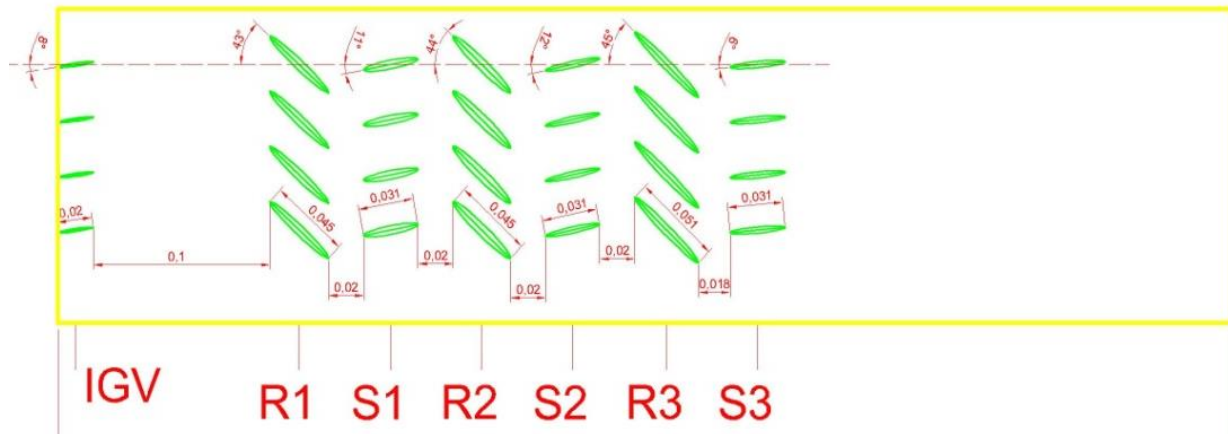


Figure 3-11: Modelled MIT GTL-LS3 compressor geometry (dimensions in m)

Table 3-1: Parameters used for simulating surge of MIT-GTL LS3 compression system

Mean Diameter R (m)	$S_c(m^2)$	$V_p(m^3)$	$L_1(m)$	$L_E(m)$
0.287	0.0662	9.66	0.86	0.44
U (m/s)	$L_{compressor}(m)$	Rotation speed (rpm)	$L_c(m)$	N_{stage}
78	0.67	2600	1.97	3.5
m	τ	ρ	l_c	B
1	0.003901	1.185	8.24	1.017

3.4.2 Low-Speed Axial-Centrifugal Compressor

For this geometry, Dumas [6] placed a generic centrifugal compressor impeller immediately downstream the MIT-GTL LS3 compressor, scaling the impeller in size and rotation speed to geometrically and aerodynamically match the upstream axial compressor. The impeller blades have a chord length of 0.224 m and stagger angle of 31.6 degree. A radial vaneless diffuser is placed at the exit of the impeller to form a simple centrifugal stage. The layout is illustrated in Figure 3-12. The parameters used for the surge simulations with the same inlet atmospheric conditions as Dumas [6] are given in Table 3.2. As a fictional compressor geometry, only CFD surge data is available from Dumas [6].

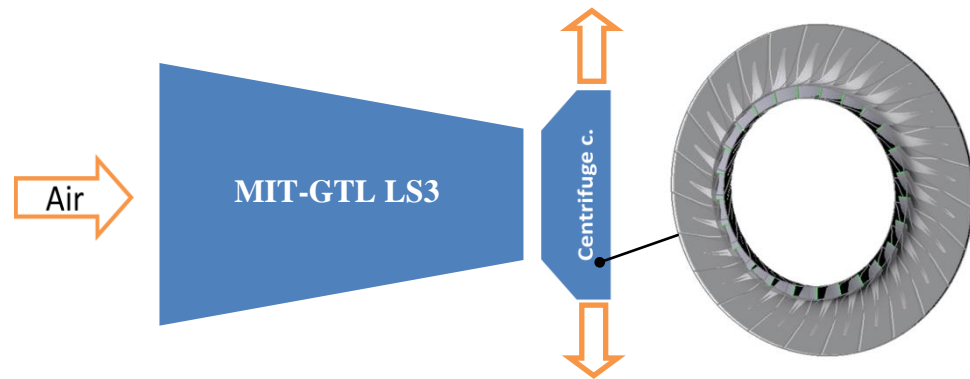


Figure 3-12 : Schematic of low-speed axial-centrifugal compressor

Table 3.2: Parameters used for simulating surge of axial-centrifugal compression system

Mean Diameter R (m)	$S_c(m^2)$	$V_p(m^3)$	$L_1(m)$	$L_E(m)$
0.287	0.0662	3.66	0	0
U (m/s)	$L_{compressor}(m)$	Rotation speed (rpm)	$L_c(m)$	N_{stage}
78	1.05	2600	1.05	4.5
m	τ	ρ	l_c	B
1	0.005495	1.185	3.659	1.7

3.4.3 High-Speed Compressor

The last geometry is a high-speed (transonic) two-stage industrial compressor, consisting of a mixed flow compressor stage with a rotor and two stators followed by a centrifugal compressor impeller and a radial vaneless diffuser that was used by Dumas to replace a pipe diffuser in the original geometry. Figure 3-13 shows a layout of the compressor passages and Table 3.3 gives the parameters used for the surge simulations with the same inlet atmospheric conditions as Dumas [6]. Only CFD surge data is available from Dumas [6] for this compressor.

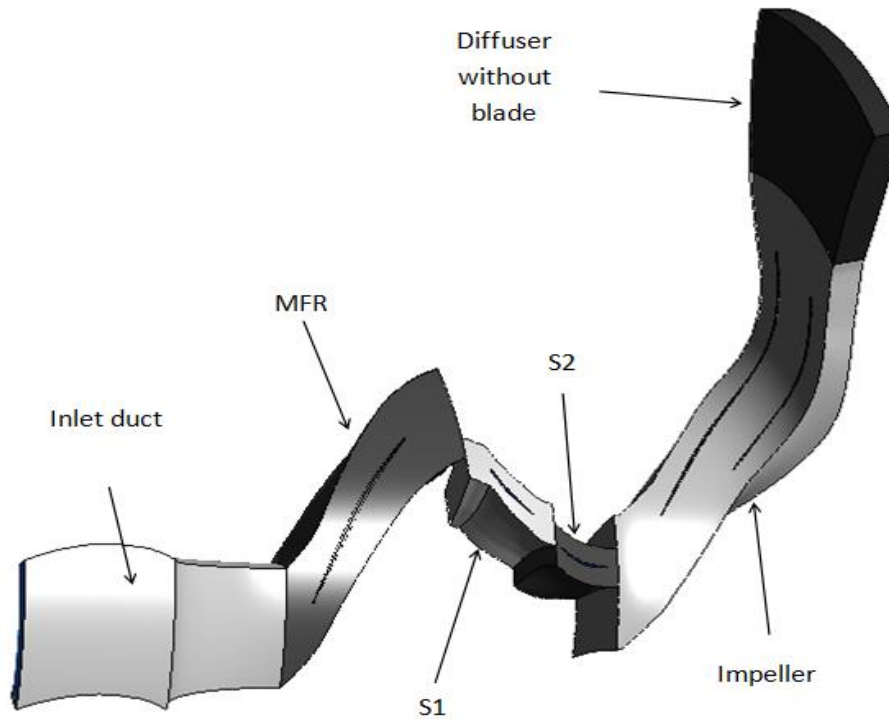


Figure 3-13: Layout of high-speed compressor[6]

Table 3.3: Parameters used for simulating surge of high-speed compression system

Mean Diameter R (m)	$S_c(m^2)$	$V_p(m^3)$	$L_i(m)$	$L_E(m)$
0.064	0.0010278	0.09	0	0
$U(m/s)$	$L_{compressor}(m)$	Rotation speed (rpm)	$L_c(m)$	N_{stage}
314	0.521	46946	0.521	2.5
m	τ	ρ	l_c	B
1	0.002	1.185	8.141	0.43

3.5 Surge Simulation Procedure

This section describes the surge simulation procedure using the proposed method. The procedure is consists of the following steps:

- 1) Compute all the basic parameters needed to run the model from the geometry of the compression system. Obtain the best possible polynomial curve fit of the total-to-static speedline matching all regions for which there is data, starting with the stable flow region.

- 2) Run the model at a low K_T value, such that the throttle line intersects the stable region of the compressor speedline as shown in Figure 3-14(a) and the pressure rise and flow coefficients converge without fluctuation to a stable value as illustrated in Figure 3-14(b).

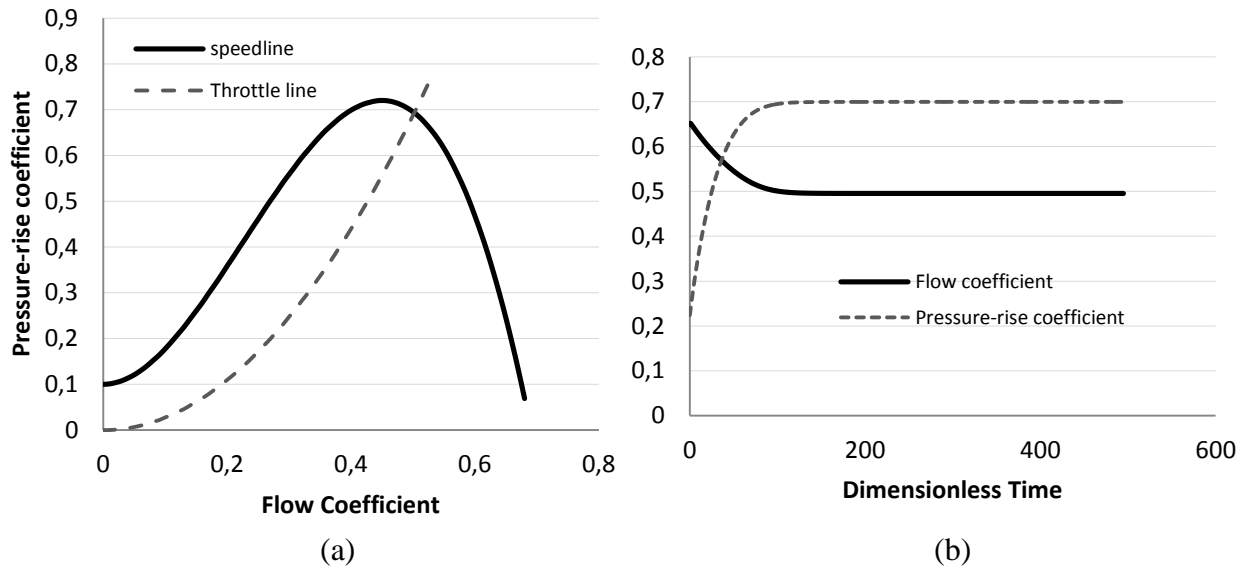


Figure 3-14: Operating point on speedline (a) and convergence history (b) for a stable value of K_T

- 3) Repeat Step 2 with gradual increase in the value of K_T until the stall point is reached. Near and at this critical (stall) K_T value, the time history of the pressure rise and flow coefficients will exhibit decaying oscillation as shown in Figure 3-15.

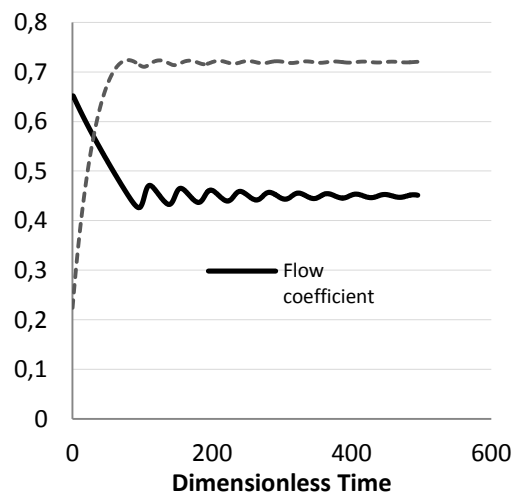


Figure 3-15: Convergence history for K_T near or at critical value (stall point)

- 4) Increase K_T beyond the critical value and run the model. This will bring the system to surge and the pressure rise and flow coefficients will exhibit large sustained temporal variations as shown in Figure 3-16.

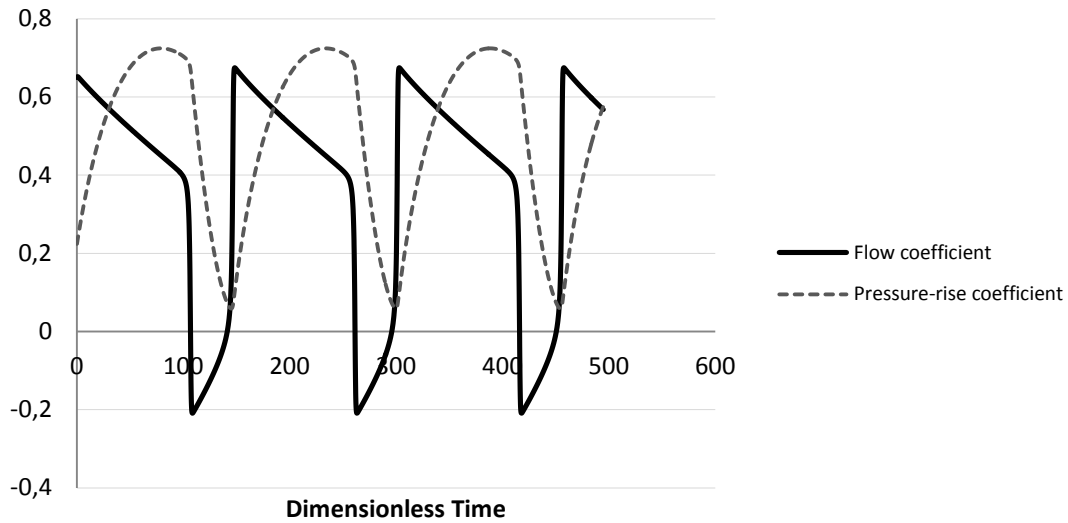


Figure 3-16: Convergence history for K_T beyond critical value (surge)

- 5) Use the temporal variations of pressure rise and flow coefficients obtained in Step 4 to calculate the pressure fluctuation at an inquiry point inside the compressor according to the procedure laid out in Section 3.2.4.

CHAPTER 4 RESULTS

This chapter presents the results of the simulations for the three compressors described in Section 3.4., comparing them with available experimental and computational data. Finally, a short parametric study is carried out on two compressor geometries to assess the effect on the surge prediction of the uncertainty in speedline shape and of neglecting the compressibility effect in a high-speed compressor.

4.1 Low-Speed Axial Compressor (MIT-GTL LS3)

4.1.1 Surge Cycle Prediction for Compressor

Figure 4-1 shows the best fit of the cubic function speedline in the form of equation (3.19) to the experimentally measured speedline segments given by Protz [28]. The model was run with the parameters given in Table 3.1 using a 0.2 ms time resolution. The value of K_T to achieve surge was 9.2 and the resulting surge cycle is compared with the experimentally measured cycle from Protz [28] in Figure 4-2. The corresponding predicted temporal variations in total-to-static pressure rise and flow coefficients are given in Figure 4-3.

One can observe from Figure 4-2 that the predicted surge cycle matches the measured cycle reasonably well both in shape and amplitude of oscillations in pressure rise and flow coefficients. Figure 3-10 indicated that the left and right curve of the limit cycle seem to follow the reversed-flow and stable segments of speedline, respectively, with the highest and lowest pressure coefficient delimited by the speedline as well. This last observation can indeed be used for estimating the value of ψ_{c0} in equation (3.19) if the approximate pressure fluctuation lower limit of the surge cycle is known. As such, one can infer that the discrepancy in the left and right curve of the surge cycle between the model and test data is linked to the discrepancy in the modelled and real speedline in Figure 4-1.

The only temporal measurement made by Protz are the hot-wire traces at different circumferential locations shown in Figure 4-4, which are equivalent to the flow coefficient except that the hot wire cannot distinguish between forward and reversed flow. However, one can see that the shape on the forward flow of the cycle is similar to the predicted flow coefficient variation in Figure 4-3

and the surge cycle oscillation frequency deduced from the predicted (1.09 Hz) and measured data (1.17 Hz) are very close.

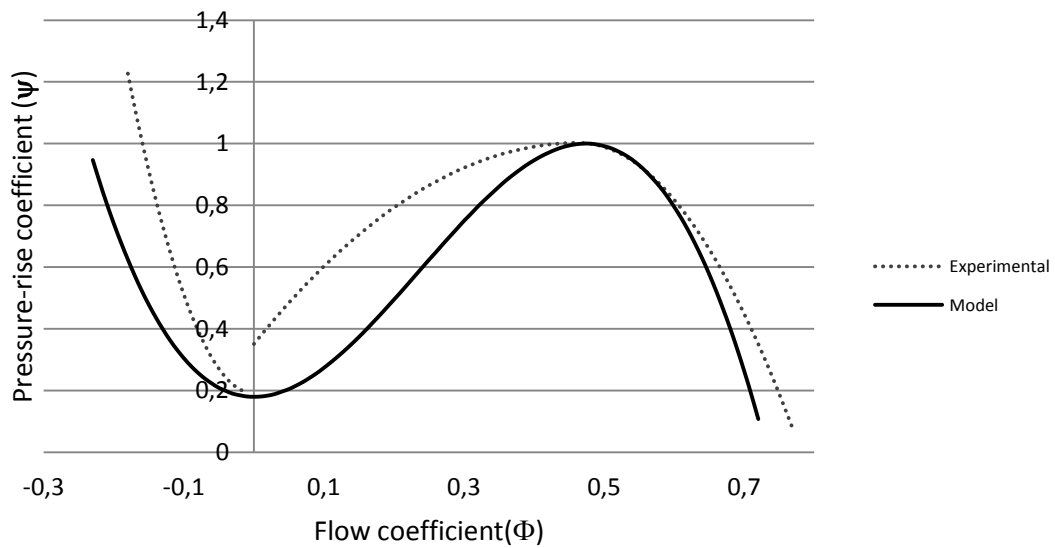


Figure 4-1: Comparison of modelled speedline against experimental equivalent from Protz [28] for MIT-GTL LS3 compressor

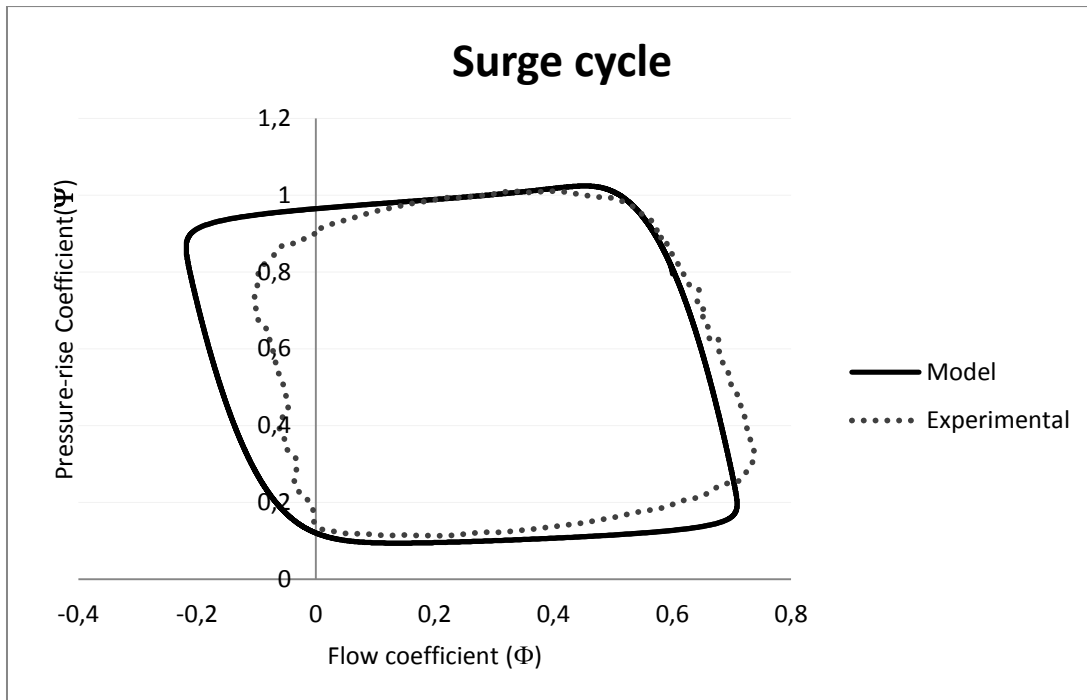


Figure 4-2: Predicted versus measured surge cycles for MIT-GTL LS3 compressor

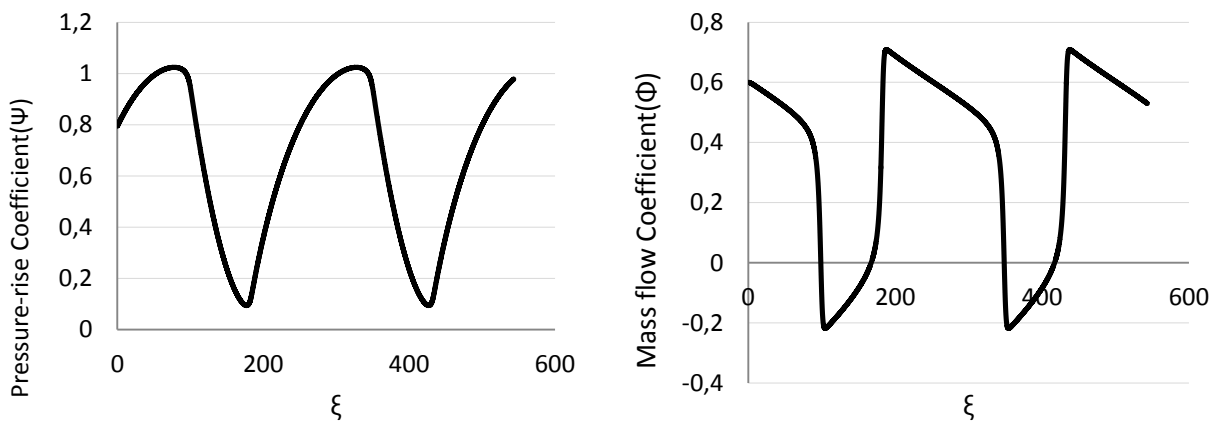


Figure 4-3: Predicted temporal variations in pressure rise and mass flow coefficients for MIT-GTL LS3 compressor (surge cycle frequency: 1.09 Hz)

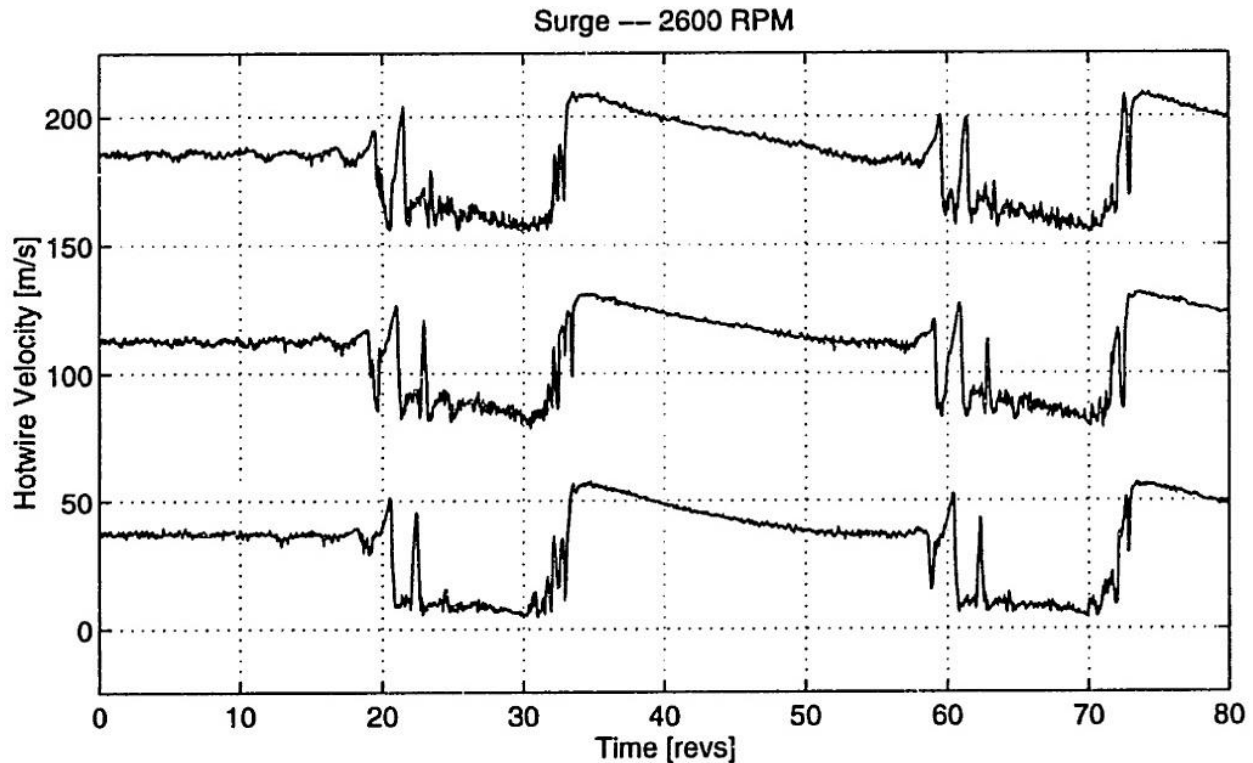


Figure 4-4: Hot-wire velocity traces during surge cycle measured by Protz [28] (surge cycle frequency: 1.17 Hz)

4.1.2 Pressure Fluctuations Inside Compressor

Since test data was not taken inside the MIT-GTL LS3 compressor by Protz [28], we must rely on the CFD predictions by Dumas [6] to evaluate the capability of the proposed method to predict pressure oscillation within the compressor. However, Dumas [6] did not simulate the exact MIT-GTL LS3 compression system. First, in the absence of exact blade 3-D shapes, he approximated the blade geometry. Second, for reasons related to numerical issues and computational time consideration, he did not incorporate the inlet and exit ducts in his simulations. However, in trying to keep the B parameter at 1, he had to reduce the plenum volume (V_p) from 9.66 m^3 to 3.66 m^3 . As such, the model used for the analytical simulation must be changed to match Dumas' numerical experiment for a fair comparison with his CFD predictions, namely changing the value of the l_c parameter from 8.24 to 2.35 and refitting the modelled cubic function speedline to match

the speedline simulated in CFD by Dumas [6] for his geometry, which only includes the stable flow range ending at the stall point, as shown in Figure 4-5. The value of ψ_{c0} for the modelled speedline is chosen to be the same as in Figure 4-1. As shown in Figure 4-6, the surge cycle predicted by the model matches reasonably well that obtained with CFD by Dumas [6] except for a small discrepancy in the reversed flow region given the lack of CFD speedline data for cubic speedline curve fitting in this region.

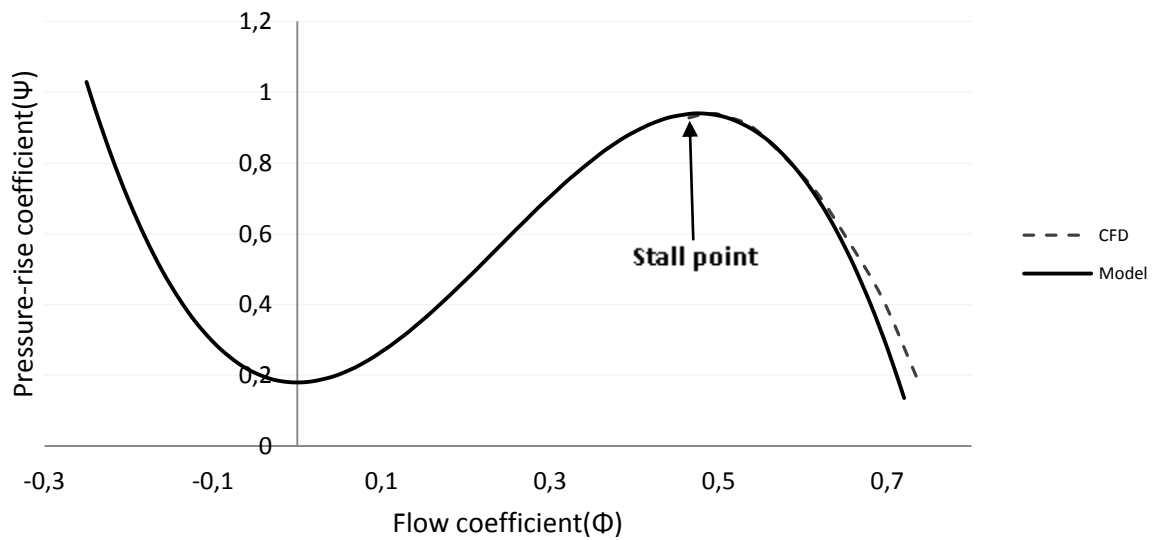


Figure 4-5: Comparison of modelled speedline against CFD equivalent from Dumas [6] for MIT-GTL LS3 compressor

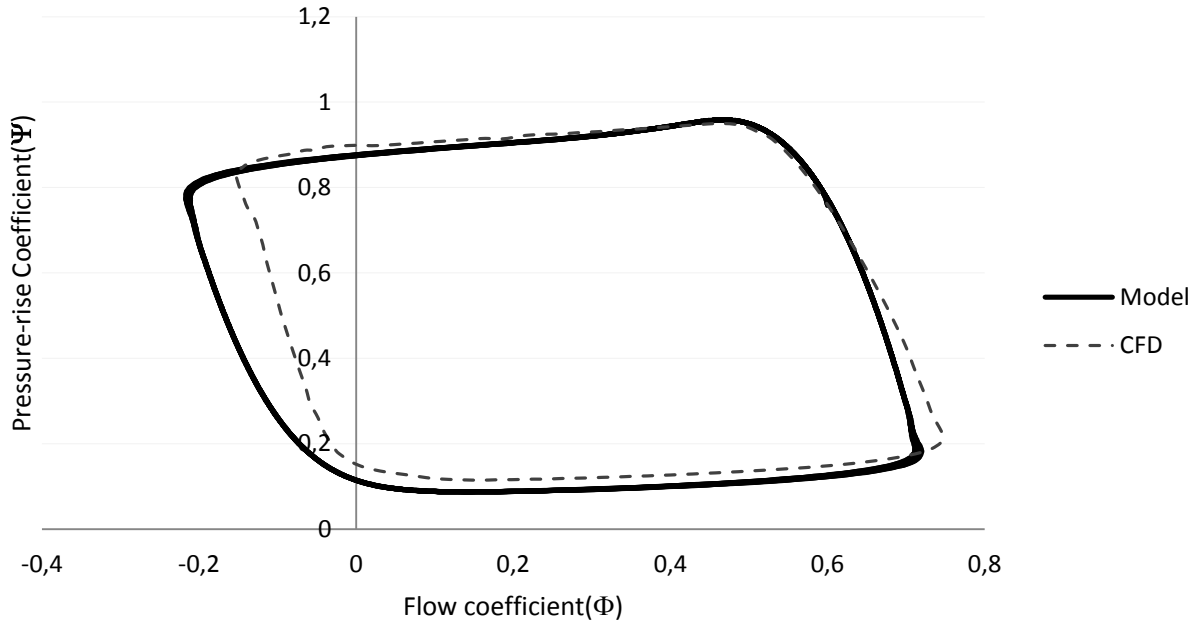


Figure 4-6: Surge cycles predicted by model versus CFD [6] for MIT-GTL LS3 compressor with no ducts and $V_p = 3.66 \text{ m}^3$

Figure 4-7 compares the time evolution of pressure rise and flow coefficients as predicted by the model and by Dumas' CFD simulations [6]. For both parameters, the match is very good in shape, amplitude and frequency.

With the surge cycle prediction for the whole compressor validated, one can proceed with predicting the pressure oscillation inside the compressor. In his case, the only pressure fluctuation data inside the compressor provided by Dumas [6] for this configuration is between the second and third stage (i.e. between Stator 2 and Rotor 3). Figure 4-8 shows plots the static-to-static pressure rise characteristic for the last stage in comparison with the total-to-static characteristic of the entire compressor. The characteristic for the last stage was obtained by dividing the static-to-static pressure rise of the three-stage compressor (total-to-static pressure rise plus inlet dynamic head, i.e. $\Psi_c + \frac{1}{2}\Phi^2$) by three through supposing the same static pressure rise for each stage. The inertia parameter τ for the last stage is calculated to be 0.00354342. Application of equation (3.20) with the data in Figures 4-7 and 4-8 gives the pressure fluctuation at the desired location (S2/R3) shown in Figure 4-9, which matches fairly well with the CFD prediction. This comparison validates the approach laid out in Section 3.2.4.

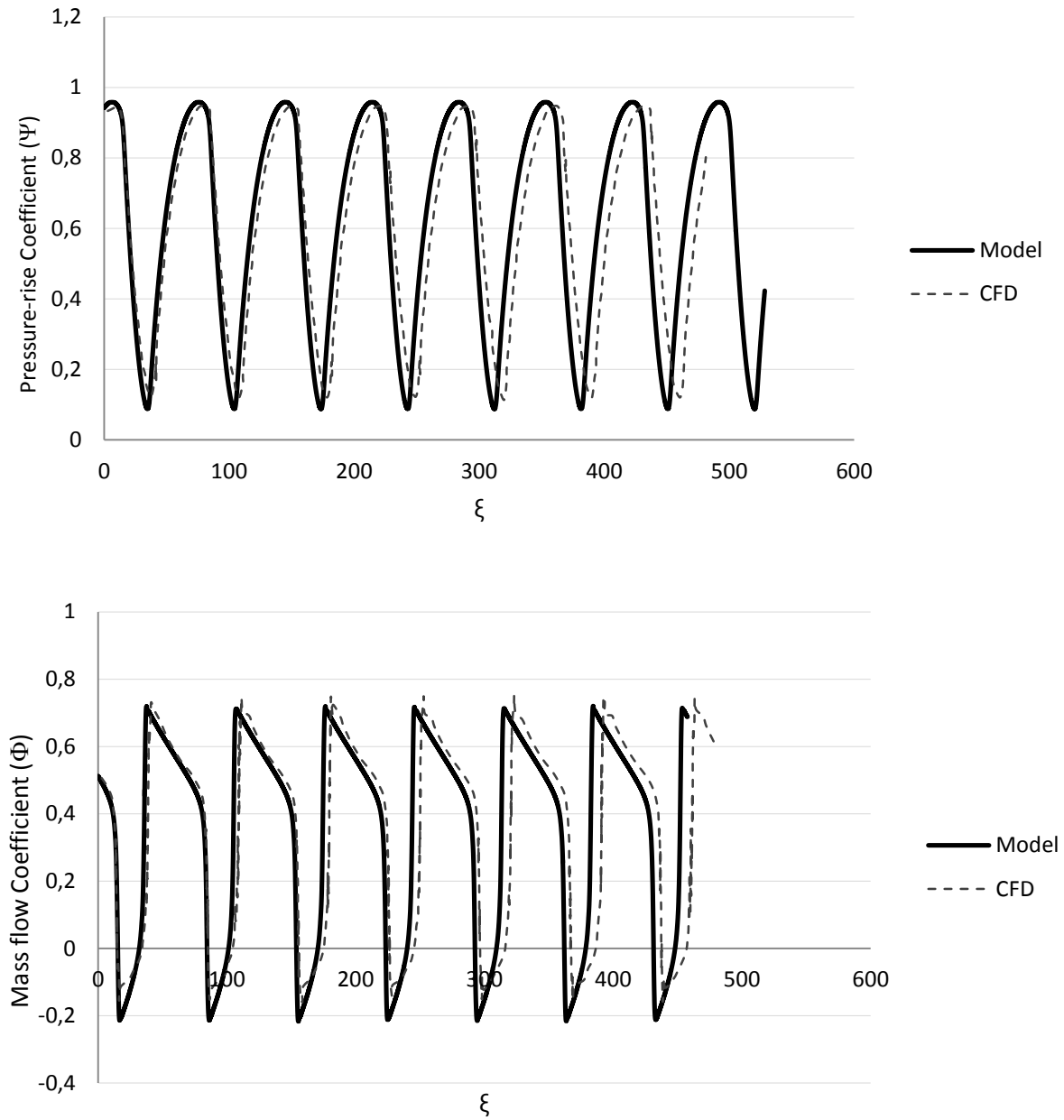


Figure 4-7: Fluctuation in pressure rise and mass flow coefficients predicted by model (3.91 Hz) versus CFD (3.88 Hz) [6] for MIT-GTL LS3 compressor with no ducts and $V_p = 3.66 \text{ m}^3$

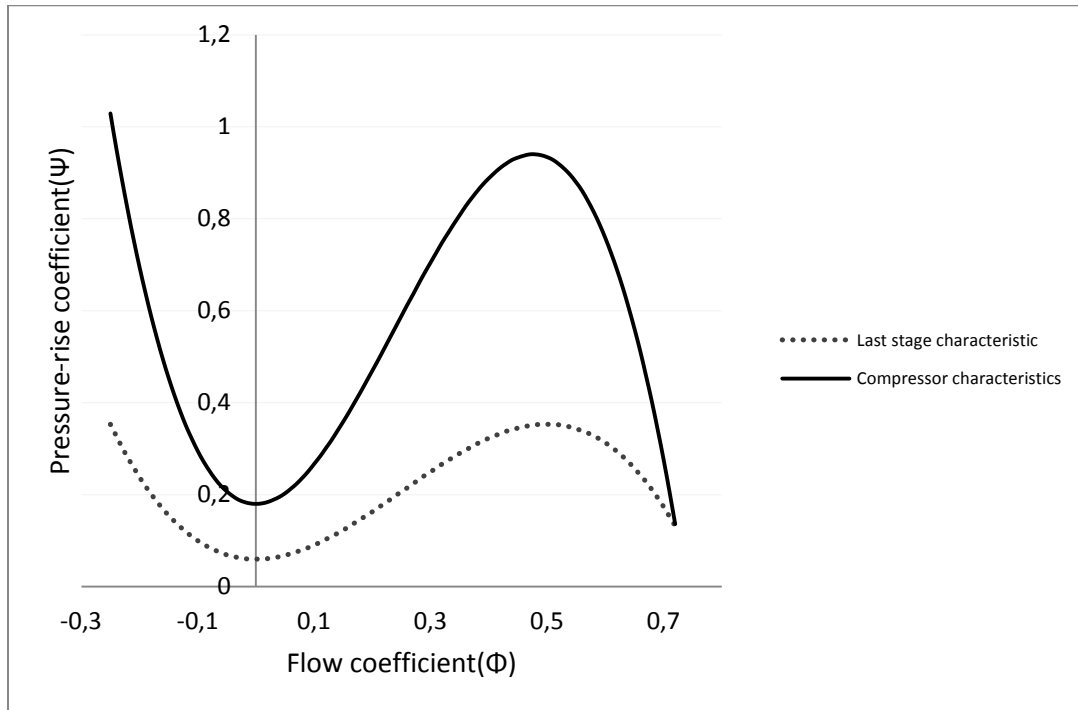


Figure 4-8: Modelled pressure rise characteristics for last stage versus entire MIT-GTL LS3 compressor

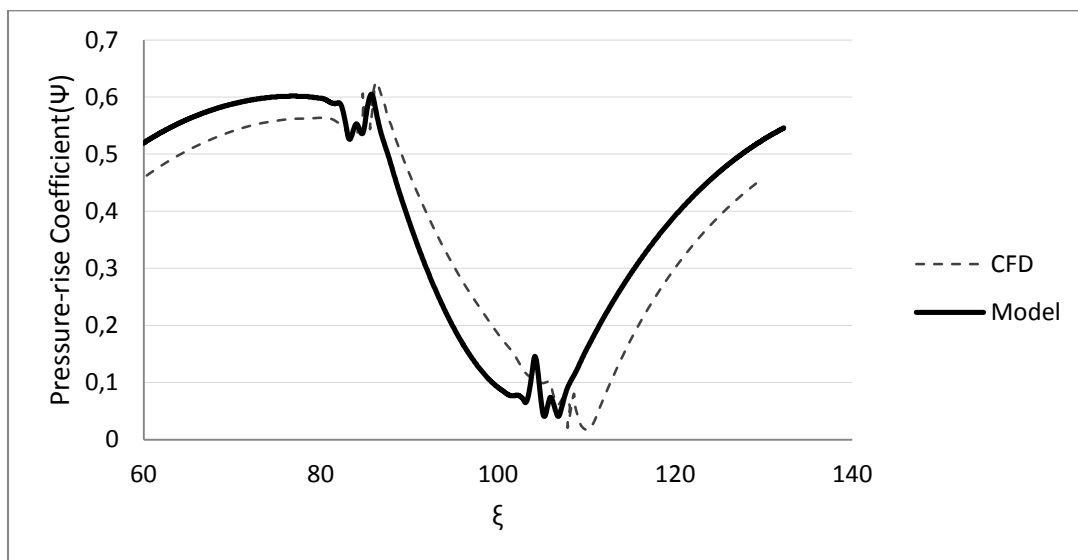


Figure 4-9: Temporal variation of the pressure rise coefficient between stages 2 and 3 of MIT-GTL LS3 compressor during a surge cycle as predicted by the model and by CFD [6].

4.2 Low-Speed Axial-Centrifugal Compressor

4.2.1 Surge Cycle Prediction for Compressor

Figure 4-10 shows the best fit of the cubic function speedline in the form of equation (3.19) to the speedline predicted by Dumas [6] for the axial centrifugal compressor using compressible CFD simulations. It is noted that the fit is not perfect and is only based on a short speedline available in the stable flow range. The value of ψ_{c0} is estimated from the surge cycle predicted by Dumas [6]. The model was run with the parameters given in Table 3.2 using a time resolution of 0.2 ms. Surge was obtained at a K_T value of 36 similar to that of Dumas [6]. The resulting surge cycle is compared with his CFD prediction in Figure 4-11. The surge cycle comparison is quite good despite the uncertainty in the modelled speedline, which bodes well for the robustness of the proposed cubic polynomial speedline model of equation (3.19). Figure 4-12 compares the temporal variation of pressure rise and flow coefficients as predicted by the model and by CFD. The model predictions compares very well with CFD in both shape and amplitude of the two parameters with just a little discrepancy in fluctuation frequency (1.53 Hz versus 1.78 Hz)

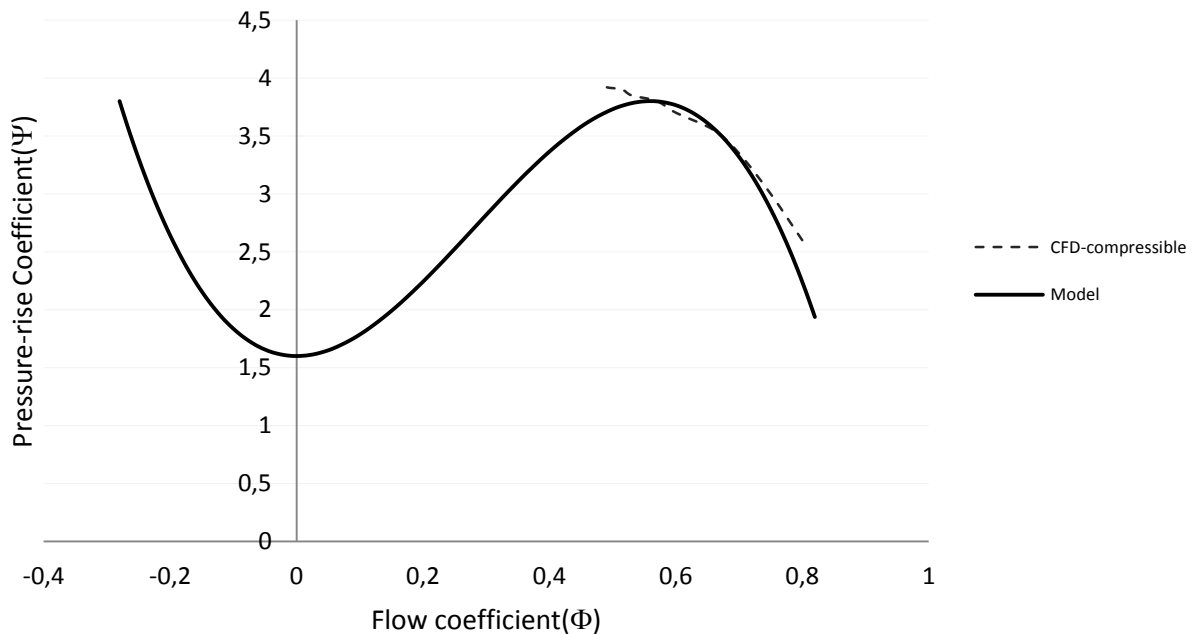


Figure 4-10 : Comparison of modelled speedline against CFD equivalent from Dumas [6] for low-speed axial-centrifugal compressor

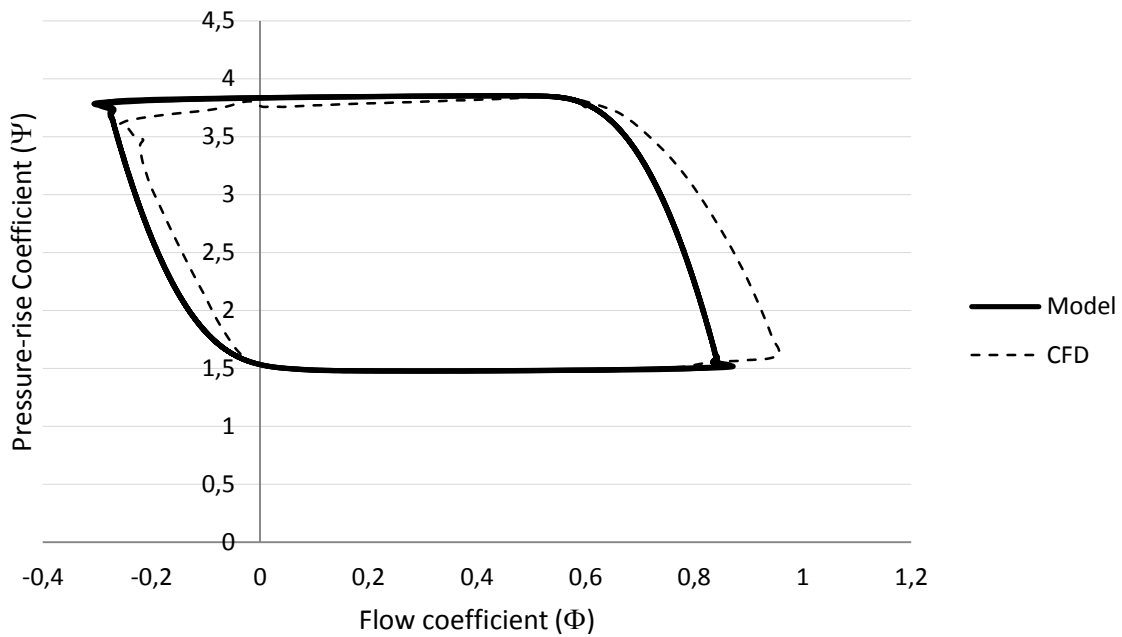


Figure 4-11: Surge cycles predicted by model versus CFD [6] for low-speed axial-centrifugal compressor

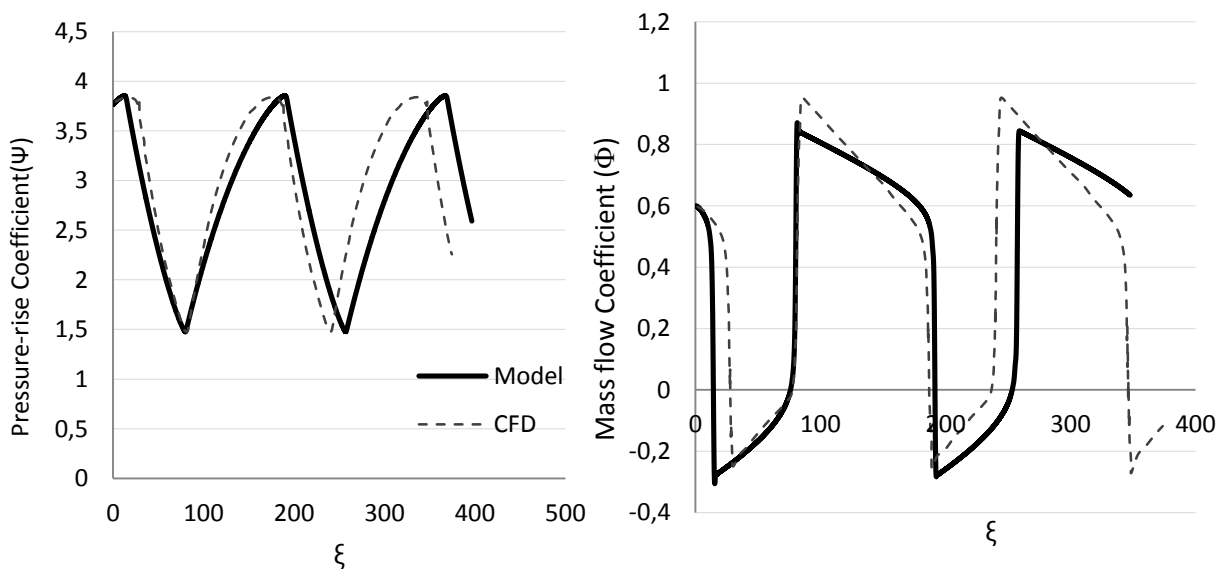


Figure 4-12: Fluctuation in pressure rise and mass flow coefficients predicted by model (1.53 Hz) versus CFD (1.78 Hz) [6] for low-speed axial-centrifugal compressor

4.2.2 Pressure Fluctuations Inside Compressor

Although pressure fluctuation prediction inside the compressor was not given by Dumas [6] for this geometry, this section presents the results of the exercise in predicting the pressure fluctuation at a location between the axial compressor and centrifugal (radial) compressor using the proposed model. Figure 4-13 plots the static-to-static pressure rise characteristic for the centrifugal compressor in comparison with the total-to-static characteristic of the entire compressor and of the axial part. The static-to-static characteristic for the radial compressor was obtained by deducting the total-to-static speedline of MIT-GTL-LS3 from that of the overall compressor. The inertia parameter τ for this stage is calculated to be 0.011076643. Application of equation (3.20) with the data in Figures 4-12 and 4-13 gives the pressure fluctuation at the desired location as shown in Figure 4-14.

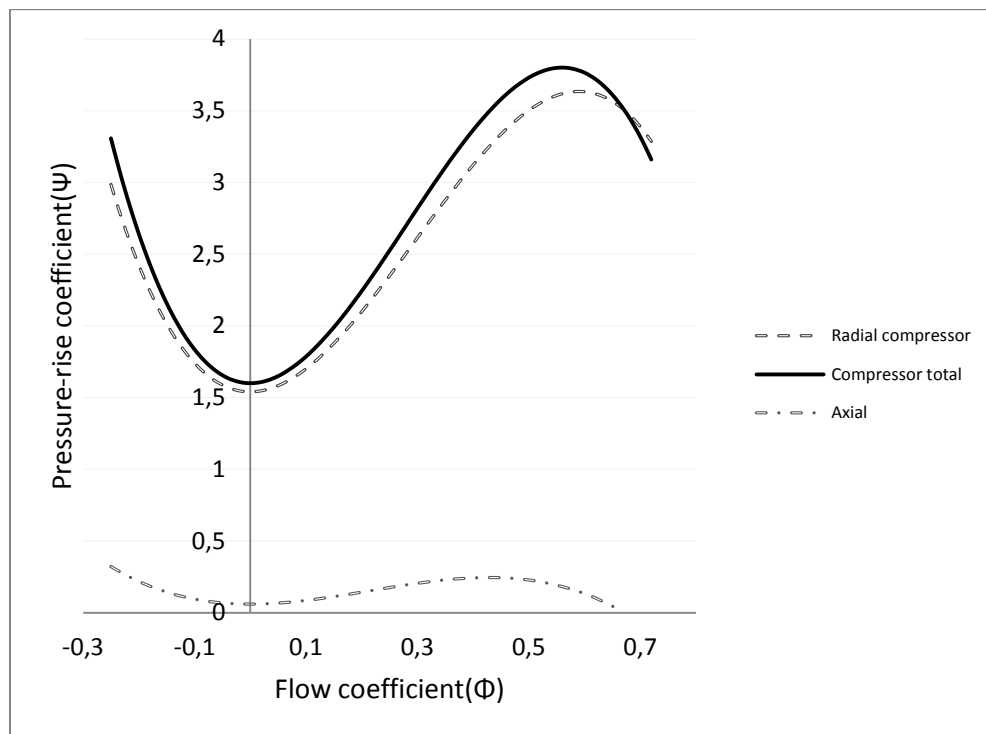


Figure 4-13: Modelled pressure rise characteristics for low-speed axial-centrifugal compressor and its axial and radial components

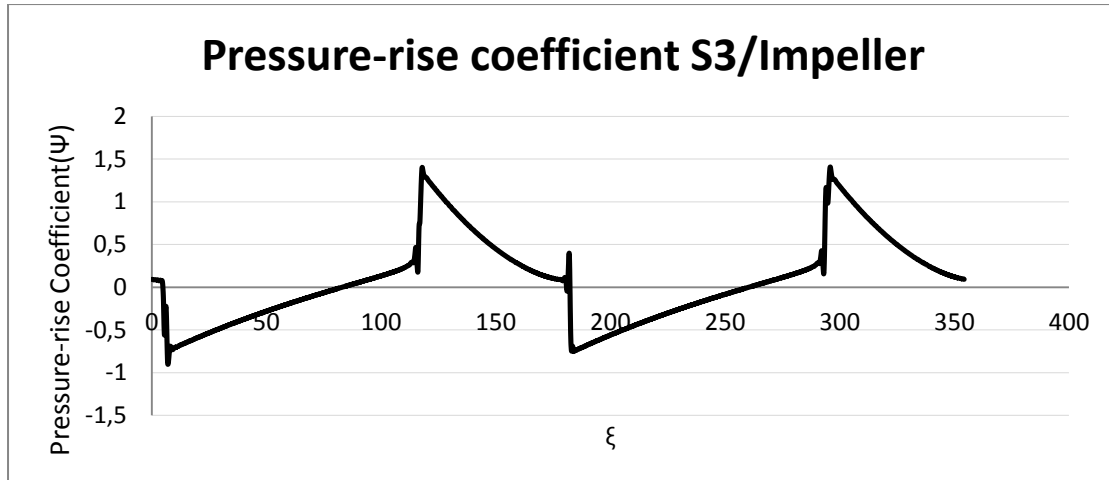


Figure 4-14: Predicted temporal variation of the pressure rise coefficient between axial and centrifugal components of low-speed axial-centrifugal compressor.

4.3 High-Speed Compressor

Unfortunately, there are no speedline data, neither experimental nor computational available for this compressor. However, as mentioned previously in Section 4.1.1, Figure 3-10 indicated that the left and right side of the limit cycle seem to follow the reversed-flow and stable operation segment of the speedline. As such, the cubic function speedline shape was estimated based on the surge cycle as given by Dumas[6] as shown in Figure 4-15. The model was run with the parameters given in Table 3.3 using a time resolution of 0.2 ms. Surge was obtained at a K_T value of 700, similar to the value of Dumas[6]. The resulting surge cycle in Figure 4-16 shows a fairly good match in fluctuation amplitude of pressure and flow coefficients with the CFD surge cycle, although with a larger difference in shape on the right side of the surge cycle very likely due to the inaccurate modelling of the speedline shape in the stable range condition. The same observation can be drawn in term of shape and amplitude from comparing the temporal variation of pressure rise and flow coefficients predicted by the model and by CFD, as shown in Figure 4-17. As for the fluctuation frequency, the discrepancy (12 Hz versus 10.61 Hz) is larger than in previous compressor but still reasonable.

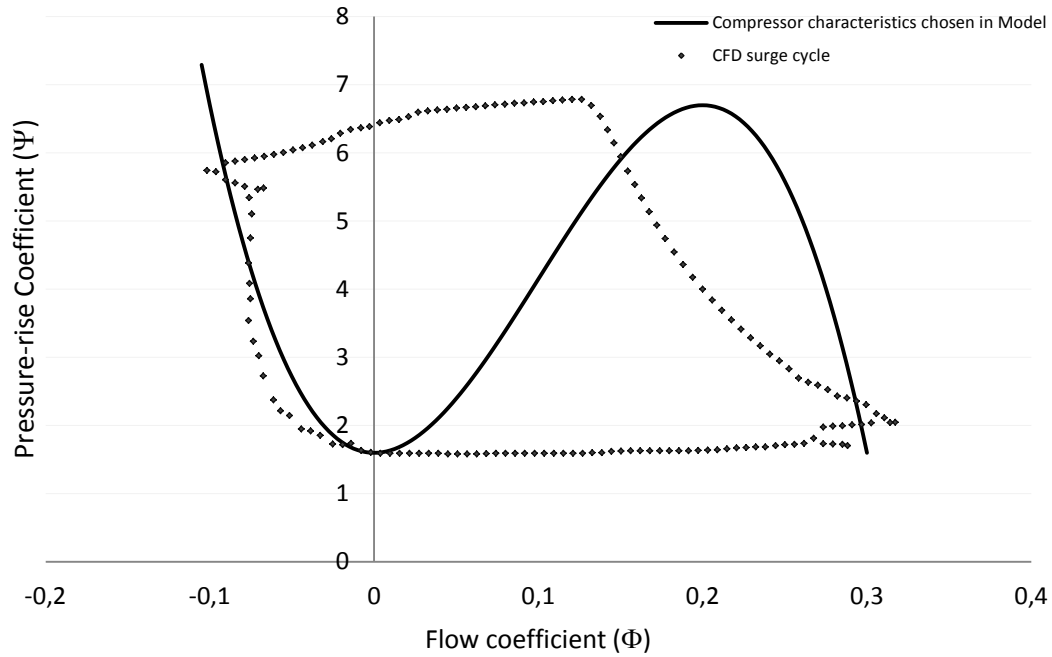


Figure 4-15: Estimation of cubic speedline based on surge cycle predicted by CFD from Dumas [6] for high-speed compressor

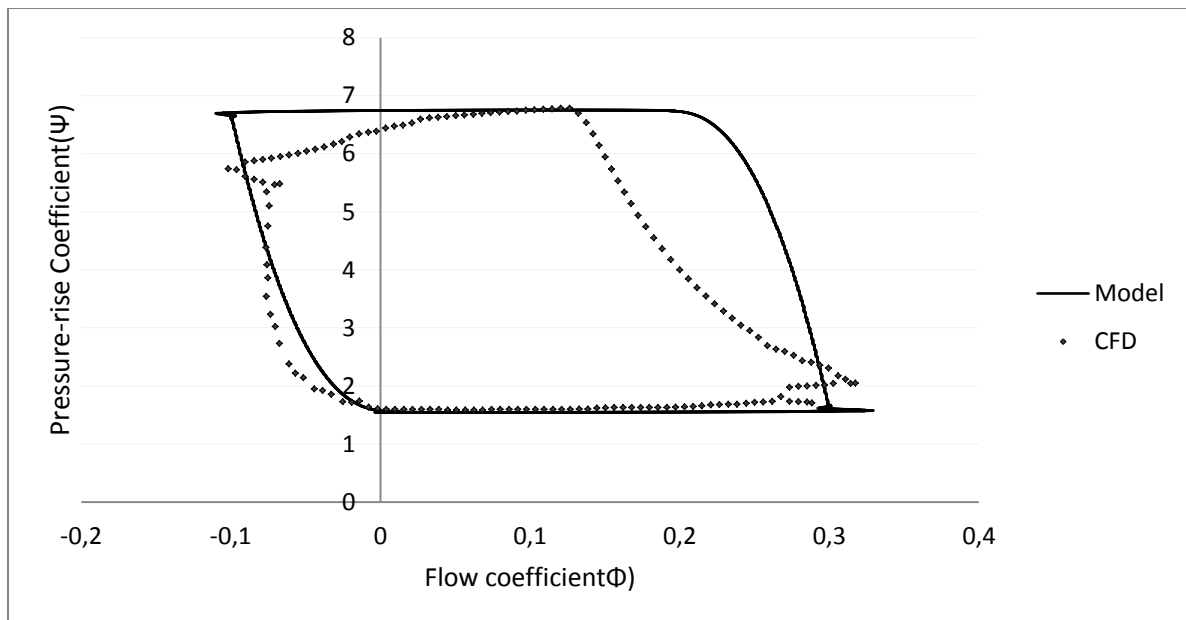


Figure 4-16: Surge cycles predicted by model versus CFD [6] for high-speed compressor

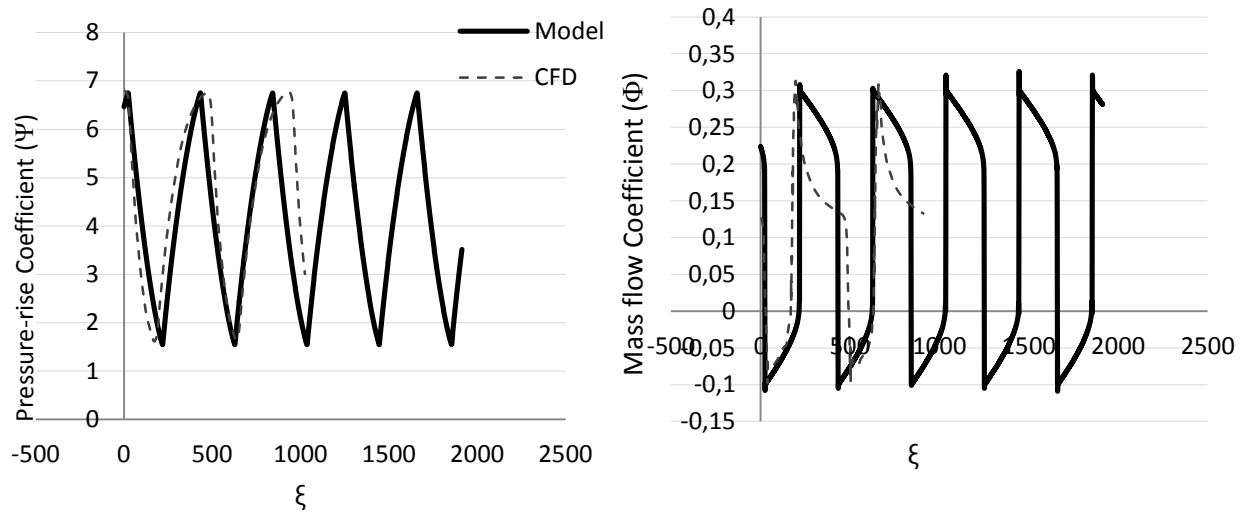


Figure 4-17: Fluctuation in pressure rise and mass flow coefficients predicted by model (12 Hz) versus CFD (10.61 Hz) [6] for high-speed compressor

4.4 Assessment of Speedline Shape and Density Effect

The results in Sections 4.1 through 4.3 for the three compressor geometries show that for a model that takes just a few minutes to set up and run, the results are quite good in terms of predicting surge cycle shape, oscillation amplitudes and frequency. However, the approximate nature of the speedline shape and the incompressibility assumption may be potentially problematic for using this model on real compressors. This section presents the results of two brief parametric studies, one on the low-speed axial compressor geometry to evaluate the effect of changing speedline shape, and the other on the effect of using different density, on the model's predictions.

4.4.1 Sensitivity of Model to Speedline Shape

The results from Sections 4.1.2, 4.2 and 4.3 indicate that fairly good surge predictions can be obtained even when the speedline shape is not well known, particularly its unstable part, for which the modelled speedline on equation (3.19) depends on the value of ψ_{c0} . However, in these cases, an adequate estimate of ψ_{c0} was possible through CFD surge cycle predictions. The question is how would the predictions be affected by uncertainty in the speedline shape from lack of a priori knowledge of the value of ψ_{c0} .

Figure 4-18 plots the surge cycle predictions for the low-speed axial compressor using the same run parameters as in Section 4.1.1 but with three different speedline shapes based on different values of ψ_{c0} . It confirms the previous observation that the shape of the reversed flow and stable parts of the speedline determines the predicted surge cycle. Thus, the modelled speedline will have a direct impact on the amplitude of predicted the pressure and mass flow fluctuations. However, with the right part of the speedline (modelled from the known stable pressure-rise characteristics), the results in Figure 4-18 show that even a large variation in the guessed value of ψ_{c0} would not change the amplitude of mass flow oscillations much and would not prevent the method from achieving the order-of-magnitude prediction accuracy in pressure fluctuation amplitude.

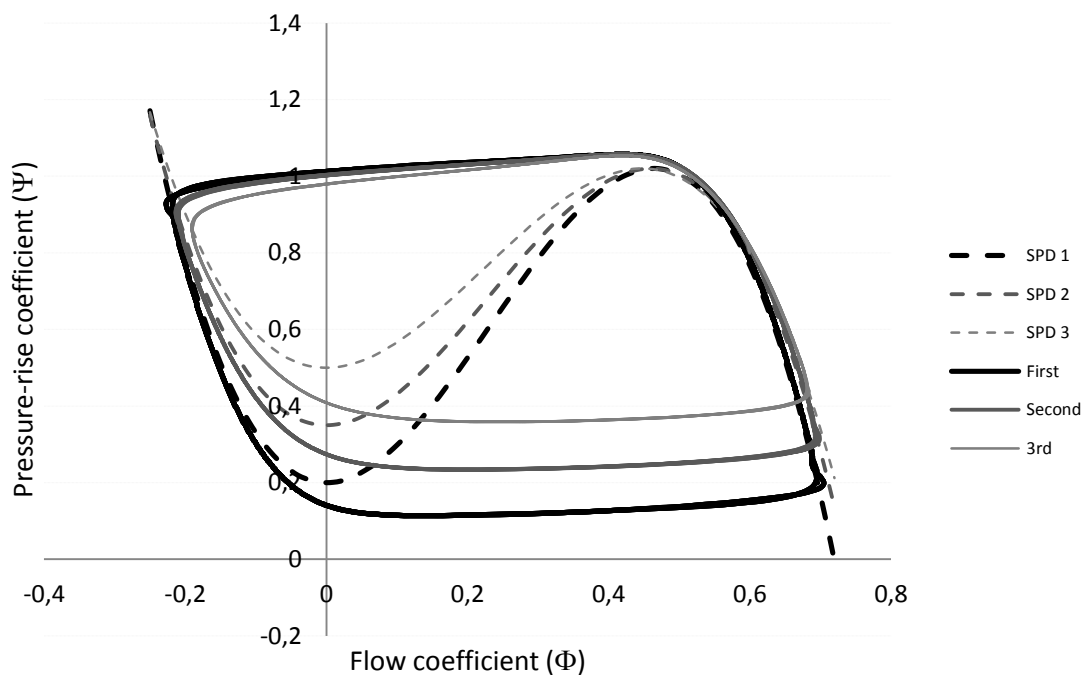


Figure 4-18: Effect of speedline shape on surge cycle predictions for MIT-GTL LS3 compressor

4.4.2 Sensitivity of Model to Density

For a high-speed compressor with significant compressibility effect, the use in the model of the inlet density with an incompressible assumption may be questionable. Figure 4-19 plots the predicted pressure rise and flow coefficients fluctuations for the high-speed compressor geometry

resulting from using different density values, namely the lowest density (calculated from static pressure and temperature at the inlet), the highest density (calculated from the compressor exit conditions) and an in-between value. The pressure rise and flow coefficients are calculated with a common density value making this equivalent to comparing the fluctuations in dimensional pressure rise and meridional velocity. The results show that, while the predicted fluctuation frequency is not affected by the density, the pressure and mass flow fluctuation amplitudes are inversely proportional to the density. However, this means that using the inlet (lowest) density will always give the highest fluctuation amplitude and thus provide the most conservative estimate.

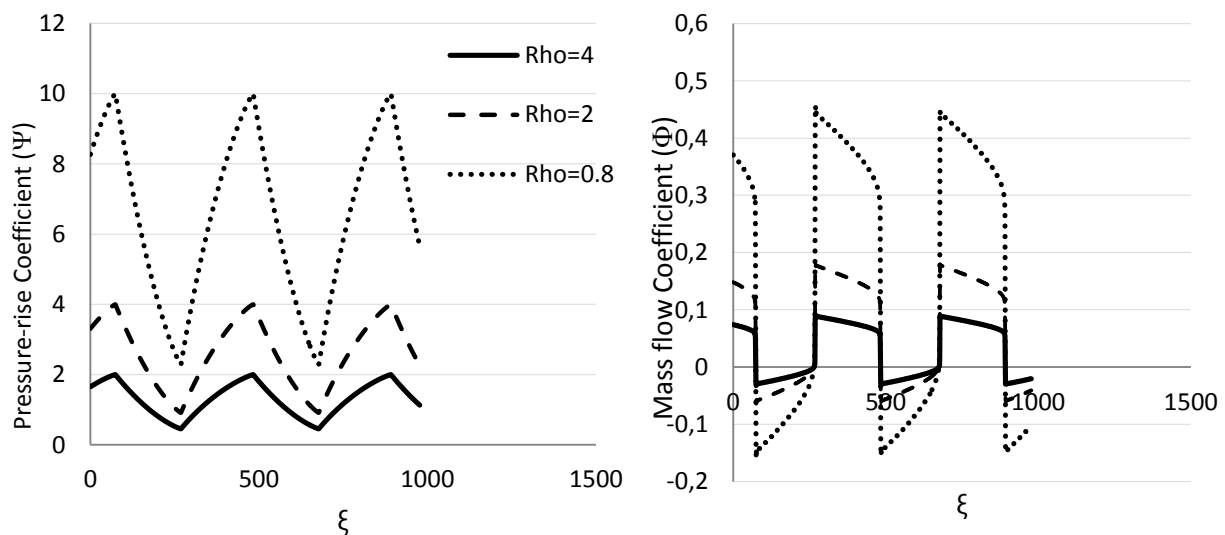


Figure 4-19: Effect of density on surge fluctuation prediction for high-speed compressor

CHAPTER 5 CONCLUSION AND RECOMMENDATIONS

A simple method has been developed in this project for simulating surge in a generic multi-stage compressor and obtaining an estimate of the pressure fluctuations at any desired location within the compressor. The method is built upon a simple analytical lumped-parameter model based on steady pressure rise characteristics and fluid inertia in the compressor coupled with 1-D model for downstream components proposed over three decades ago to simulate surge in low-speed axial compressors. Through this work, this model is shown to be also applicable to non-axial compressor and the same steady pressure rise and fluid inertia effect is applied to subsections of the compressor to easily predict pressure oscillations inside the compressor once the surge prediction for the entire compressor has been obtained.

The incompressible model was applied on three different compressor geometries ranging from a three-stage low-speed (incompressible) axial compressor with available test and CFD simulation surge data to an industrial high-speed two-stage (highly compressible) non-axial compressor with CFD simulations surge data. The results show that this simple model that is easy and fast to set up and run performs quite well in predicting the surge cycle shape, fluctuation amplitude and frequency for the overall compressor and for a location inside the compressor (at least on the low-speed axial compressor) in spite of uncertainty in speedline shape estimation and the incompressibility assumption.

Unfortunately, insufficient data has prevented verification of the proposed model for predicting pressure fluctuation inside high speed compressors with important compressibility effect. Thus, the recommended future work includes:

- Validation of model on high-speed compressors with test data
- If necessary, implement modification to the model to better take into account compressibility effects, such as what density should be used in estimating the inertia effect of subsections to calculate fluctuations inside high-speed compressors.
- Change the modelled cubic characteristics to another format that is more flexible in matching known characteristics shape
- Change the model formulation to avoid using an average flow inertia parameter

BIBLIOGRAPHY

- [1] J. Dahl, "Jet engine(File:Jet engine.svg)," 2014.
- [2] (2015). *Aircraft engine*. Available: http://www.electron.rmutphysics.com/science-news/index.php?option=com_content&task=view&id=738&Itemid=4&limit=1&limitstart=3)
- [3] I. Day, "Active suppression of rotating stall and surge in axial compressors," *Journal of Turbomachinery*, vol. 115, pp. 40-47, 1993.
- [4] J. M. Haynes, G. J. Hendricks, and A. H. Epstein, "Active stabilization of rotating stall in a three-stage axial compressor," *Journal of Turbomachinery*, vol. 116, pp. 226-239, 1994.
- [5] E. M. Greitzer, "Surge and rotating stall in axial flow compressors—Part I: Theoretical compression system model," *Journal of Engineering for Gas Turbines and Power*, vol. 98, pp. 190-198, 1976.
- [6] M. Dumas, "Développement d'une méthode de simulation de pompage au sein d'un compresseur multi-étagé," École Polytechnique de Montréal, 2013.
- [7] H. Emmons, C. Pearson, and H. Grant, "Compressor surge and stall propagation," *Trans. ASME*, vol. 77, pp. 455-469, 1955.
- [8] E. M. Greitzer, "Surge and rotating stall in axial flow compressors—Part II: experimental results and comparison with theory," *Journal of Engineering for Gas Turbines and Power*, vol. 98, pp. 199-211, 1976.
- [9] W. Du and O. Léonard, "Numerical simulation of surge in axial compressor," *International Journal of Rotating Machinery*, vol. 2012, 2012.
- [10] K. Hansen, P. Jorgensen, and P. Larsen, "Experimental and theoretical study of surge in a small centrifugal compressor," *Journal of Fluids Engineering*, vol. 103, pp. 391-395, 1981.
- [11] I. Day, "Axial compressor performance during surge," *Journal of Propulsion and Power*, vol. 10, pp. 329-336, 1994.

- [12] F. Moore, "A theory of rotating stall of multistage axial compressors: part I—small disturbances," *Journal of Engineering for Gas Turbines and Power*, vol. 106, pp. 313-320, 1984.
- [13] F. K. Moore and E. M. Greitzer, "A theory of post-stall transients in axial compression systems: Part I—Development of equations," *Journal of Engineering for Gas Turbines and Power*, vol. 108, pp. 68-76, 1986.
- [14] E. Greitzer and F. Moore, "A theory of post-stall transients in axial compression systems: part II—application," *Journal of Engineering for Gas Turbines and Power*, vol. 108, pp. 231-239, 1986.
- [15] L. P. Bonnaure, "Modelling high speed multistage compressor stability," Massachusetts Institute of Technology, 1991.
- [16] Z. S. Spakovszky, "Applications of axial and radial compressor dynamic system modeling," Massachusetts Institute of Technology, 2000.
- [17] H. J. Weigl, "Active stabilization of rotating stall and surge in a transonic single stage axial compressor," Massachusetts Institute of Technology, Dept. of Aeronautics and Astronautics, 1997.
- [18] M. Morini, M. Pinelli, and M. Venturini, "Development of a one-dimensional modular dynamic model for the simulation of surge in compression systems," *Journal of Turbomachinery*, vol. 129, pp. 437-447, 2007.
- [19] A. Hale and M. Davis, "Dynamic turbine engine compressor code DYNTECC—theory and capabilities," *AIAA Paper No. AIAA-92-3190*, 1992.
- [20] W. T. Cousins, "The dynamics of stall and surge behavior in axial-centrifugal compressors," Virginia Polytechnic Institute and State University, 1997.
- [21] G. D. Garrard, "ATEC: The Aerodynamic Turbine Engine Code for the Analysis of Transient and Dynamic Gas Turbine Engine System Operations," 1995.
- [22] S. Niazi, "Numerical simulation of rotating stall and surge alleviation in axial compressors," Ph.D. 9978412, Georgia Institute of Technology, United States -- Georgia, 2000.

- [23] S. Guo, H. Chen, X. Zhu, and Z. Du, "Numerical simulation of surge in turbocharger centrifugal compressor - Influences of downstream plenum," in *ASME 2011 Turbo Expo: Turbine Technical Conference and Exposition, GT2011, June 6, 2011 - June 10, 2011*, Vancouver, BC, Canada, 2011, pp. 1897-1908.
- [24] M. Vahdati, G. Simpson, and M. Imregun, "Unsteady flow and aeroelasticity behavior of aeroengine core compressors during rotating stall and surge," *Journal of Turbomachinery*, vol. 130, p. 031017, 2008.
- [25] S. Koff and E. Greitzer, "Stalled flow performance for axial compressors. I-Axisymmetric characteristic," in *29th International Gas Turbine Conference and Exhibit*, 1984.
- [26] S. G. Koff, "Stalled flow characteristics for axial compressors," Massachusetts Institute of Technology, 1983.
- [27] R. N. Gamache, "Axial Compressor Reversed Flow Performance," DTIC Document 1985.
- [28] J. M. Protz, "Nonlinear active control of rotating stall and surge," Massachusetts Institute of Technology, 1997.
- [29] R. Gamache and E. Greitzer, "Reverse flow in multistage axial compressors," *Journal of Propulsion and Power*, vol. 6, pp. 461-473, 1990.
- [30] A. H. J. Eastland, "An experimental investigation of compressor performance in rotating stall," Massachusetts Institute of Technology, 1982.
- [31] K. Magnus, *Vibrations*: Blackie & Son, 1965.

APPENDICES

APPENDIX A – NUMERICAL IMPLEMENTATION

This appendix describes the method used to solve the three equations of the Moore-Greitzer model [13] for aerodynamic instabilities of the compressor, namely equations (3.12), (3.13) and (3.20):

$$\Psi(\xi) = \psi_c(\Phi(\xi) - Y_{\theta\theta}) - l_c \frac{d\Phi}{d\xi} - mY_\xi + \frac{1}{2a}(2Y_{\xi\theta\theta} + Y_{\theta\theta\theta}) \quad (3.12)$$

$$\Psi(\xi) = \frac{1}{2\pi} \int_0^{2\pi} \psi_c(\Phi(\xi) - Y_{\theta\theta}) d\theta - l_c \frac{d\Phi}{d\xi} \quad (3.13)$$

$$\frac{\partial \Psi}{\partial \xi} = \frac{1}{4B^2 l_c} \left(\Phi(\xi) - \sqrt{\frac{2\Psi(\xi)}{K_t}} \right) \quad (3.18)$$

To solve the above of system of coupled partial differential equations which include derivatives which are third order in θ , but first order in time, the Galerkin method of nonlinear mechanics [31] is used to reduces the order of the equations in θ . The resulting set of ODE is solved using Matlab-Simulink.

A.1 Galerkin Procedure

In the Galerkin procedure, the solution to the differential equation is represented by a suitable sequence of basic functions. Fourier series or spectral methods are examples of this procedure. A fully nonlinear Galerkin [31] approximation of the Moore-Greitzer compressor model had been derived for this analysis. The simplest wave representation is chosen as:

$$Y = WA(\xi)\sin(\theta - r(\xi)) \quad (A.1)$$

where Y is a single harmonic function of unknown amplitude $A(\xi)$ and phase angle $r(\xi)$. By substituting equation (A.1) in equation (3.13), the residual can be formulated[13].

By substituting the characteristic described in equation (3.19) and using the f_0 propagation speed described in Moore [12].

$$r = \xi f_0 \quad (\text{A.2})$$

$$f_0 \equiv \frac{1/2}{1+ma} \quad (\text{A.3})$$

And using the convenience variable $J(\xi) \equiv A^2(\xi)$, the final equations are:

$$l_c \frac{d\Psi}{d\xi} = \frac{1}{4B^2} \left[\Phi - \sqrt{\frac{2\Psi}{K_T^2}} \right] \quad (\text{A.4})$$

$$\frac{d\Phi}{d\xi} = \left[-\frac{\Psi - \psi_{c0}}{H} + 1 + \frac{3}{2} \left(\frac{\Phi}{W} - 1 \right) \left(1 - \frac{1}{2} J \right) - \frac{1}{2} \left(\frac{\Phi}{W} - 1 \right)^3 \right] \frac{H}{l_c} \quad (\text{A.5})$$

$$\frac{dJ}{d\xi} = J \left[1 - \left(\frac{\Phi}{W} - 1 \right)^2 - \frac{1}{4} J \right] \frac{3aH}{(1+ma)W} \quad (\text{A.6})$$

These are the final equations that the circumferentially averaged flow coefficient (Φ), pressure-rise coefficient (Ψ) and squared amplitude of angular variation (J), as functions of dimensionless time (ξ). This ODE system can now be solved.

A.2 Solution in Simulink

Matlab-Simulink was chosen to numerically solve the nonlinear ODE system represented by equation (A.4), (A.5) and (A.6) system and for post-processing the results. The ability to choosing easily different solver in the prepared interface of the software is one of the advantages of the Simulink. Furthermore, Simulink is more suitable for any future work implicating flow control.

The first step is to define the governed equations and parameters as a function file in Matlab. This function will be called in Simulink to be solved. Figure A-1 shows the graphical layout of the Simulink program used. A time step and solver need to be chosen. Depending on the case, the choice of solver may have to be changed to get converged results. The time step can be easily changed in each simulation. Choosing a suitable time step may help avoid numerical errors and will later help in calculating the frequency and post-processing the results for comparison with experimental data.

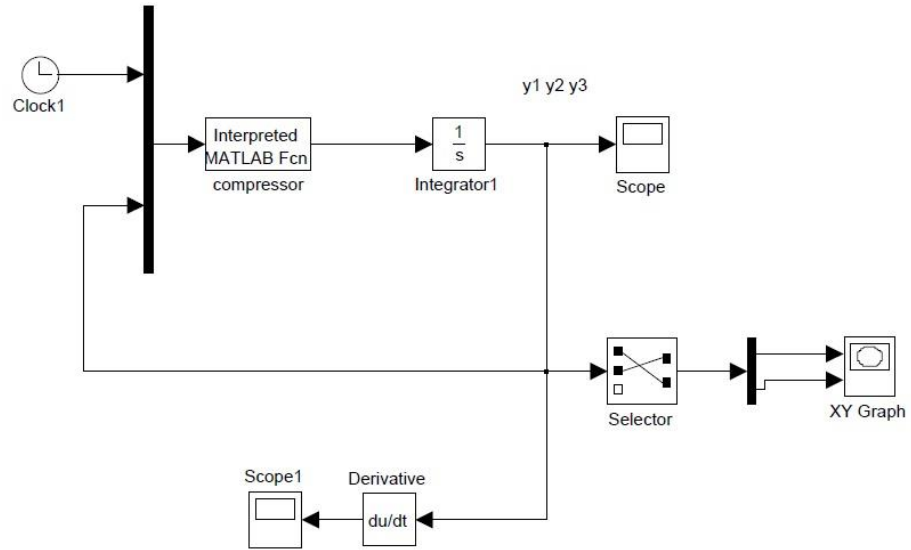


Figure A-1: Simulink blocks for solving surge ODEs

APPENDIX B – CALCULATION OF INERTIA PARAMETER

This appendix outlines the procedure used to calculate the inertia parameter τ using as example the case of the MIT-GTL LS3 compressor and the following centrifugal stage that make up the axial-centrifugal compressor. As illustrated in Figure B-1, which shows the layout of the MIT-GTL LS3 compressor with the modelled blade rows, the main simplifying assumption is that the inertia of the fluid between two blade rows is calculated with same flow angle as the upstream blade row stagger angle γ . Since the interblade row distance is treated as a part of the blade row, the multiplier parameter k in equations (3.2) and (3.3) is set to 1 and the axial gap distance is divided by the stagger angle

Table B.1 lists the values chord and stagger angles and resulting τ^* , as defined by equation (B.1) for each blade row and gap in the axial-centrifugal compressor, using $U = 78\text{m/s}$ and $R = 0.287\text{m}$. The final τ value is the average of these τ^* calculated according to equation (B.2). Finally, to find the pressure fluctuation at within the compressor from equation (3.20), the value of τ used to obtain the inertia of the last compressor section (section 2 in figure 3-6) is the sum of all τ^* contained in that section.

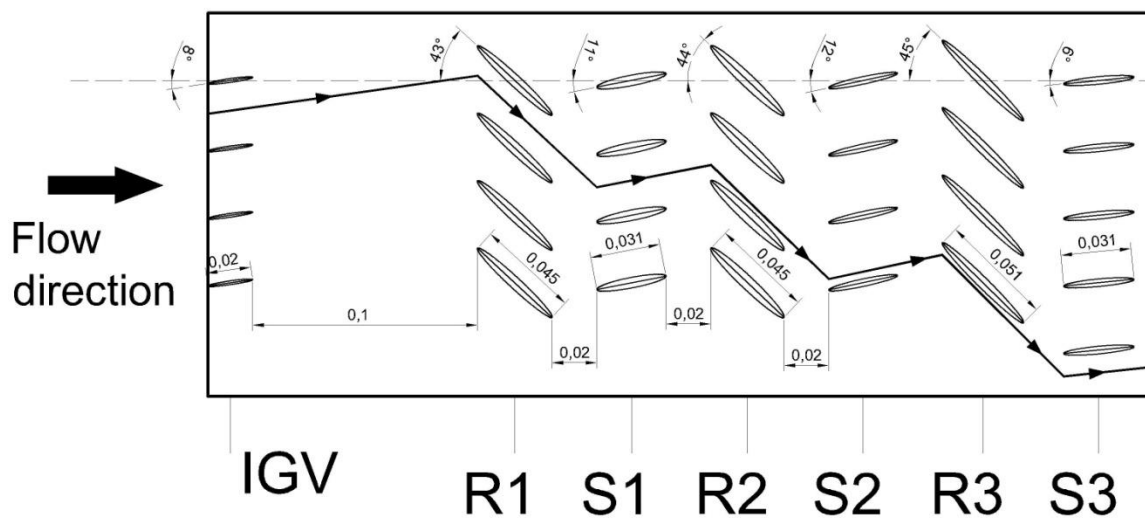


Figure B-1: Modelled flow path inside MIT-GTL LS3 compressor

$$\tau^* \equiv \frac{2kb}{U \cos(\gamma)} \quad (\text{B.1})$$

$$\tau \equiv \frac{\sum \tau^*}{N_{\text{stages}}} \quad (\text{B.2})$$

Table B-1: Inertia components associated with blade rows and gaps for axial and centrifugal compressor stages in axial-centrifugal compressor

Blading		IGV	STAGE 1	STAGE 2	STAGE 3
Rotor Chord(m)			0.045212	0.0448056	0.0506984
Rotor stagger(deg)			42.8	43.5	44.6
Rotor τ^*			0.00158	0.001583	0.00183
Stator Chord(m)		0.0200914	0.0313944	0.0312928	0.0313944
Stator stagger(deg)		8.1	11	12	5.5
Stator τ^*		0.0005	0.00082	0.00082	0.00081
Rotor-Stator gap(m)			0.01999996	0.01999996	0.01800098
Rotor-Stator Gap τ^*			0.00095	0.000974	0.00091
Inter-stage gap (m)		0.100203	0.01999996	0.01999996	
Inter-stage Gap τ^*		0.0026	0.00053	0.000536	
			Centrifugal		
Impeller chord(m)			0.224		
Impeller stagger(deg)			31.6		
Impeller τ^*			0.00674		
Diffuser Chord(m)			0.144		
Diffuser stagger(deg)			31.6		
Impeller τ^*			0.00433		